Beamforming in Integrated Sensing and Communication Systems With Reconfigurable Intelligent Surfaces

R. S. Prasobh Sankar, *Graduate Student Member, IEEE*,
Sundeep Prabhakar Chepuri, *Member, IEEE*, and Yonina C. Eldar, *Fellow, IEEE*

***Abstract*— We consider transmit beamforming and reflection pattern design in reconfigurable intelligent surface (RIS)-assisted integrated sensing and communication (ISAC) systems to jointly precode communication symbols and radar waveforms. We treat two settings of multiple users and targets. In the first, we use a single RIS to enhance the communication performance of the ISAC system and design beams with good cross-correlation properties to match a desired beampattern while guaranteeing a desired signal-to-interference-plus-noise ratio (SINR) for each user. In the second setting, we use two dedicated RISs to aid the ISAC system, wherein the beams are designed to maximize the worst-case target illumination power while guaranteeing a desired SINR for each user. We propose solvers based on alternating optimization as the design problems in both cases are non-convex optimization problems. Through numerical simulations, we demonstrate the advantages of RIS-assisted ISAC systems. In particular, we show that the proposed single-RIS assisted ISAC system improves the minimum user SINR while suffering from a moderate loss in radar target illumination power. On the other hand, the dual-RIS assisted ISAC system improves both minimum user SINR as well as worst-case target illumination power at the targets, especially when the users and targets are not directly visible to the ISAC transmitter.**

***Index Terms*— Dual function radar communication system, integrated sensing and communication, mmWave MIMO, reconfigurable intelligent surfaces, transmit beamforming.**

I. Introduction

INTEGRATED sensing and communication (ISAC) systems are envisioned to play a crucial role in 5G advanced and 6G wireless networks [1], [2], [3], [4], [5]. Dual function radar communication base station (DFBS) is an example of an ISAC system that communicates with user equipments (UEs) while using the same resources to carry out sensing tasks [6], [7], [8], [9]. The integration of communication and sensing functionalities is usually achieved by using communication waveforms to also carry out radar sensing, embedding communication symbols in radar waveforms, or designing precoders to jointly transmit communication and sensing waveforms [10], [11].

One of the main drawbacks of using radar (communication) signals to carry out both communication and sensing is the inevitable degradation in the communication (respectively, radar) performance. For example, using radar waveforms for ISAC limits the communication data rate to the order of the pulse repetition interval of the radar waveform. This issue can be alleviated by using dedicated beamformers to carry out communication and sensing functionalities [12], [13], [14]. Furthermore, even though dedicated beams are used for sensing, DFBS can exploit communication waveforms for radar sensing as well without treating it as interference as it has full knowledge of both waveforms.

Transmit beamformers in multiple input multiple output (MIMO) radar systems are typically designed to either achieve a desired beampattern at the transmitter or to maximize the illumination power at different target directions [15]. The design of transmit beamformers in [15] has been extended to ISAC systems in [12] and [13], where different beamformers for UEs and target directions are designed to guarantee a minimum signal-to-interference-plus-noise ratio (SINR) to the UEs while matching a desired beampattern at the transmitter [12] or to minimize the radar sensing Cramér-Rao lower bound [13]. In [14], the authors propose a radar priority approach, wherein the radar signal-to-noise ratio (SNR) is maximized while serving as many users as possible, each with a minimum SINR.

Large available bandwidths at mmWave frequency bands can be exploited to achieve high data rates and to obtain improved range resolution for radar sensing. Operating at mmWave frequencies is challenging due to the pathloss, which is so severe that the non-line-of-sight (NLoS) paths can be too weak to be of any practical use, preventing reliable communication or sensing. However, when the direct links to the UEs or targets are weak or absent, the aforementioned methods [12], [13], [14] will not be able to provide desired levels of radar or communication performance. To combat

Manuscript received 18 July 2022; revised 13 March 2023 and 5 July 2023; accepted 25 August 2023. Date of publication 18 September 2023; date of current version 10 May 2024. This work was supported in part by the Next Generation Wireless Research and Standardization on 5G and Beyond Project, Ministry of Electronics and Information Technology (MeitY), Government of India; and in part by the Prime Minister's Research Fellowship (PMRF), Government of India. The associate editor coordinating the review of this article and approving it for publication was X. Tao. *(Corresponding author: R. S. Prasobh Sankar.)*

R. S. Prasobh Sankar and Sundeep Prabhakar Chepuri are with the Department of Electrical Communication Engineering, Indian Institute of Science, Bengaluru 560012, India (e-mail: prasobhr@iisc.ac.in; spchepuri@iisc.ac.in).

Yonina C. Eldar is with the Department of Mathematics and Computer Science, Weizmann Institute of Science, Rehovot 7610001, Israel (e-mail: yonina.eldar@weizmann.ac.il).

Color versions of one or more figures in this article are available at https://doi.org/10.1109/TWC.2023.3313938.

Digital Object Identifier 10.1109/TWC.2023.3313938

such harsh propagation environments, an emerging technology with large two-dimensional array of passive reflectors, referred to as reconfigurable intelligent surfaces (RISs) is receiving significant attention, separately for wireless communications [16], [17], localization [18], and radar sensing [19], [20], [21], [22]. RIS is a two-dimensional array of phase shifters, which can be independently tuned from the base station. Although RISs do not have any signal processing capabilities to perform data acquisition, channel estimation, or symbol decoding, its phase profile can be designed to favorably alter the wireless propagation environment and introduce *virtual* line-of-sight (LoS) paths, which enable communication or sensing even when the direct path is blocked.

Integrating RIS into ISAC has been considered recently in several works [23], [24], [25], [26], [27], [28], [29], [30], [31], [32], [33], [34] to achieve improved per user SINR and/or sum target illumination power, especially when the direct path from the DFBS to the UEs or targets are blocked. Typically, the design of transmit beamformers (or waveforms) and the RIS phase shifts is carried out to achieve desired levels of communication and sensing performance. Usual choices of communication performance metric are SNR [23], [24], [25], [28], SINR [32], [34], sum-rate [27], [33], or multi-user interference [29], [30], [31]. Commonly used radar performance metrics are target received SNR [23], [24], [27], [28], [29], sum-SNR [34], worst-case target illumination power [25], transmit beampattern mismatch error [30], [32], direction of arrival estimation Cramér-Rao bound [31], or the interference of communication waveforms on radar [33]. Most of the aforementioned works consider relatively simple settings such as single user multiple targets [25], multiple users single target [27], [28], [29], or using only single-antenna for communications [24]. Methods designed to work with single UE often use SNR as the communication metric. However, in the presence of multiple users, it is typical to use SINR as a metric, which is a fractional function that cannot be readily handled using the solvers in [23], [24], and [25]. Similarly, methods intended to sense only a single target such as [23], [27], [28], and [29] use radar SNR as the metric. In presence of multiple targets, metrics such as worst-case target illumination power, beampattern mismatch error, or sum-radar SINR is preferred. Hence algorithms designed for handling a single target [23], [27], [28], [29] cannot be readily extended to sense multiple targets.

The most general setting of RIS-assisted ISAC systems for multiple users and targets is considered in [30], [31], [32], [33], and [34]. In [30] and [31], a single dedicated transmit waveform is used for communication and sensing. In [32], transmit beamformers and reflection coefficients are designed for an ISAC system having separate colocated subarrays for sensing and communication. Due to the close proximity of radar and communication subarrays, the signal received at the RIS will also receive a significant amount of radar waveforms, resulting in increased interference at the UEs, that is however ignored in [32]. Moreover, target sensing is not possible whenever the direct paths are blocked since the targets are directly sensed by the DFBS without any aid from the RIS.

An RIS assisted radar-communication-coexistence (RCC) system is considered in [33], where geographically separated transceivers are used for sensing and communication. However, the design of radar waveforms to achieve a certain radar performance is not considered in [33] with the study being limited to the reduction of communication interference on the radar system. In [34], the sum radar SNR due to multiple targets is used as the radar performance metric to design separate communication and sensing beamformers. Considering the sum radar SNR as a radar metric leads to scenarios with the entire power being transmitted towards one of the targets, resulting in the radar system completely missing one or more targets (see Figs. 3(a) and 3(b) in Section VI-A). Furthermore, [30], [31], [32], [33], and [34] consider a setting where RIS is not used for radar sensing. Hence, whenever the targets are not directly visible to the DFBS, it is not possible to leverage the benefit of RIS to introduce additional paths that enable reliable sensing [19].

In this paper, we focus on multi-user multi-target scenarios and propose two algorithms to circumvent the limitations in the aforementioned prior art, such as the possibility of ISAC systems missing a few targets and enabling sensing even when the direct path to the targets is absent. To this end, we form multiple beams towards all target directions by using a fairness-promoting radar metric to ensure that all the targets are illuminated. We propose to use an additional dedicated RIS to enable reliable sensing even when the direct paths to some or all of the targets are blocked. Our major contributions are summarized as follows.

A. RIS Only for Assisting Communications

In the first setting, a single RIS, referred to as comm-RIS, is solely used to enhance the communication performance. We assume that the targets and users are well separated (for example, the targets could be unmanned aerial vehicles or cars on the road whereas the users could be pedestrians walking on the sidewalk) with comm-RIS located closer to the UEs. We design the RIS phase shifts and transmit beamformers to form uncorrelated beams by matching it to a desired beampattern while ensuring a minimum received SINR for the UEs. This is a non-convex optimization problem. Therefore, we design the beamformers and phase shifts using alternating optimization by designing the transmit beamformers while keeping the RIS phase shifts fixed and vice versa. Given the beamformers, we choose comm-RIS phase shifts to maximize the SINR, which leads to a *multi-ratio fractional problem*, which is then solved using an iterative procedure based on the *Dinkelbach method* [35]. Due to the specific choice of radar and communication metrics, the proposed method also enforces fairness to all the UEs and targets.

B. Dual RIS for Both Communications and Sensing

In the second setting, we propose a dual-RIS assisted ISAC system, where we use geographically separated dedicated RISs for sensing and communication. As before, we assume that the users and targets are spatially well separated and that a single comm-RIS located close to the UEs cannot efficiently sense

the targets, hence motivating the need to use an additional RIS, referred to as radar-RIS, for sensing. Due to the fully passive nature of both RISs, we cannot form uncorrelated beams for radar sensing as before. Hence, we maximize the worst-case target illumination power while ensuring a minimum received SINR for the UEs. We solve the resulting non-convex design problem using alternating optimization. While the procedure for designing comm-RIS phase shifts is the same as in the first setting, to design the radar-RIS phase shifts, we propose a method based on semidefinite relaxation followed by Gaussian randomization. In contrast to [34], our scheme ensures that even the weakest target is illuminated so that the DFBS can reliably sense all the targets present in the scene even if the targets are not directly visible to the DFBS.

We denote the proposed alternating optimization solvers as `Proposed-D`. We also propose low-complexity solvers (referred to as `Proposed-F`) to design the comm-RIS phase shifts for both scenarios. Specifically, we formulate the comm-RIS phase shift design problem as a feasibility problem (as opposed to a more complex multi-ratio fractional problem), which we propose to solve using semidefinite relaxation (SDR). Through numerical simulations, we demonstrate the benefits of the proposed designs of RIS-assisted ISAC systems. The comm-RIS assisted ISAC system (designed using `Proposed-D`) significantly improves the fairness SINR of the communication UEs (often by about $15-20$ dB as compared to [34]) while suffering a moderate loss of about $1.5-2.5$ dB in the worst-case target illumination power as compared to systems without RIS [12]. This loss is due to the fraction of the total power sent to comm-RIS. For the dual-RIS assisted setup (designed using `Proposed-D`) with dedicated RISs for sensing and communications, due to the enhanced degrees of freedom in the design due to radar-RIS, both the fairness SINR and worst-case target illumination power are significantly improved (by about 10 dB and $15-20$ dB, respectively) as compared with an ISAC system without RIS [12], especially when all the targets are not directly visible to the DFBS. Moreover, for both scenarios, `Proposed-F` is also found to outperform the benchmark schemes albeit with a lower performance when compared to `Proposed-D`.

The remainder of the paper is organized as follows. We present the system model in Section II. We describe the performance metrics and formulate the design problems in Section III. The proposed alternating optimization solvers and their low-complexity alternatives are developed in Section IV and Section V, respectively. Numerical simulations demonstrating the performance of the proposed algorithms are presented in Section VI. We conclude the paper in Section VII.

Throughout the paper, we use lowercase letters to denote scalars and boldface lowercase (uppercase) to denote vectors (matrices). We use $(\cdot)^{\mathrm{T}}$, $(\cdot)^*$, and $(\cdot)^{\mathrm{H}}$ to denote transpose, complex conjugation, and Hermitian (i.e., complex conjugate transpose) operations, respectively. $[\mathbf{x}]_n$ or x_n denotes the n-th entry of the vector $\mathbf{x}$. We define the set of N dimensional vectors with unit modulus entries as $\Omega^N = \{\mathbf{a} \in \mathbb{C}^N : |a_i| = 1,\ i = 1,\ldots,N\}$ and the set of all $M \times M$ positive semidefinite matrices are denoted by $\mathbb{S}_+^M$.

II. System Model

Consider an RIS-assisted MIMO ISAC system with a DFBS communicating with K single antenna users and simultaneously sensing T point targets in the far field of the DFBS and RIS. The DFBS has a uniform linear array (ULA) with M antennas, which transmits both communication symbols and radar waveforms.

In this paper, we consider two different settings. In the first setting, the RIS (referred to as comm-RIS) empowers only the communication part of ISAC, wherein the transmit signal reaches the UEs via a direct and an indirect path through the RIS and the transmit signal reaches the target only via a direct path. In the second setting, we have a dual-RIS setup with one RIS dedicated to sensing (referred to as radar-RIS) and one to communications (referred to as comm-RIS). In the second setting, in addition to both users and targets receiving signals via the direct path, users (targets) also receive signal through the comm-RIS (respectively, the radar-RIS).

RIS can introduce virtual paths to sense targets that are not in direct line-of-sight (LoS) with the DFBS (i.e., similar purpose as comm-RIS) and can also be used to enable co-existence in ISAC systems and localize targets. In an RIS-assisted sensing system, the angle at the DFBS can be estimated by applying any one of the many direction estimation techniques such as Bartlett beamforming or Capon beamforming on the received echo signals, and the angles at the radar-RIS can be estimated by using a codebook-based scheme [26]. However, in this paper, we focus on transmit beamforming, wherein the beams are designed towards known directions of interest.

We assume that the targets and users are spatially well separated with comm-RIS (radar-RIS) located closer to the UEs (respectively, the targets) as illustrated in Fig. 1. Hence, the wireless links between comm-RIS (radar-RIS) and the targets (respectively, the UEs) are very weak, and effect of the corresponding wireless channels on the system can be safely ignored. The first setting is well suited when the targets are directly visible to the DFBS via a direct path, like for aerial surveillance or for environments with limited scattering. On the other hand, the second setting is suited for scenarios where the direct path to the targets is blocked or very weak, e.g., localization of cars or pedestrians in an urban setting, i.e., for environments with rich scattering.

A. Downlink Transmit Signal Model

Let $\mathbf{w}_n = [w_1[n],\ldots,w_M[n]]^{\mathrm{T}} \in \mathbb{C}^M$ denote the discrete-time baseband radar waveforms at time instance n. We define the discrete-time complex baseband downlink communication symbols transmitted to the K UEs as $\mathbf{d}_n = [d_1[n],\ldots,d_K[n]]^{\mathrm{T}} \in \mathbb{C}^K$. We precode $\mathbf{d}_n$ with the communication beamformer $\mathbf{C} = [\mathbf{c}_1,\mathbf{c}_2,\ldots,\mathbf{c}_K] \in \mathbb{C}^{M\times K}$ and precode $\mathbf{w}_n$ using the sensing beamformer $\mathbf{S} = [\mathbf{s}_1,\mathbf{s}_2,\ldots,\mathbf{s}_M] \in \mathbb{C}^{M\times M}$. The precoded radar waveforms and communication symbols are superimposed and transmitted from the DFBS as

$$\mathbf{x}_n = \mathbf{C}\mathbf{d}_n + \mathbf{S}\mathbf{w}_n \in \mathbb{C}^M. \tag{1}$$

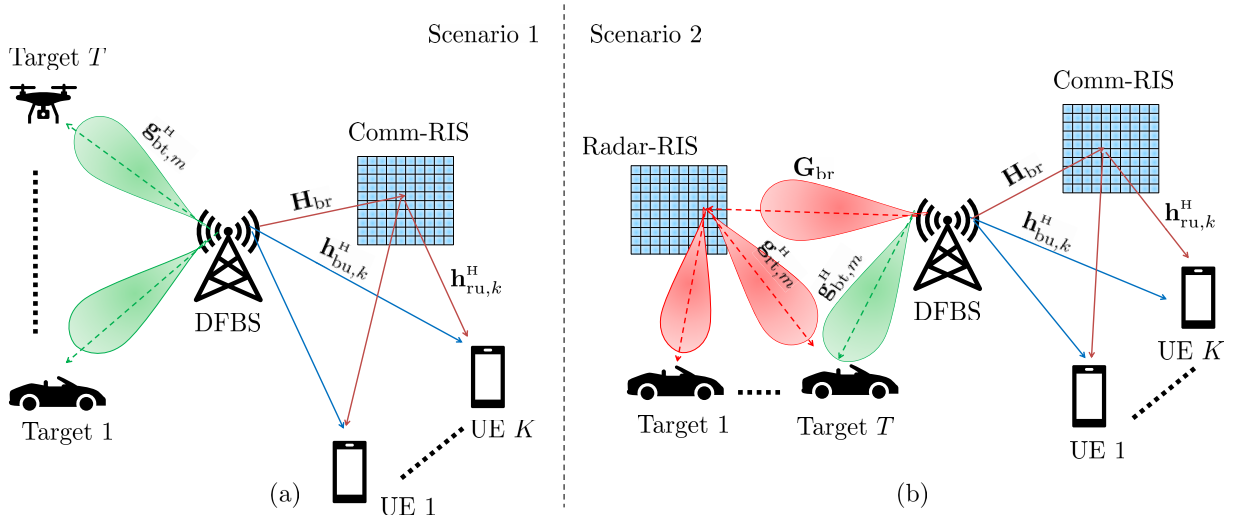

Fig. 1. System model of an RIS-assisted ISAC system. (a) RIS assists only the communication functionality. (b) Dual RISs for communications and sensing.

We assume that the UEs do not cooperate with each other and hence the communication symbols transmitted towards different UEs are assumed to be uncorrelated. We also assume that the radar and communication symbols are uncorrelated with each other and have unit power, i.e., $\mathbf{R}_d = \mathbb{E}\left[\mathbf{d}_n\mathbf{d}_n^{\mathrm{H}}\right] = \mathbf{I}_M$, $\mathbf{R}_w = \mathbb{E}\left[\mathbf{w}_n\mathbf{w}_n^{\mathrm{H}}\right] = \mathbf{I}_M$, and $\mathbb{E}\left[\mathbf{d}_n\mathbf{w}_n^{\mathrm{H}}\right] = \mathbf{0}$. Thus, the transmit signal covariance matrix $\mathbf{R} = \mathbb{E}\left[\mathbf{x}_n\mathbf{x}_n^{\mathrm{H}}\right] \in \mathbb{S}_+^M$ is given by

$$\mathbf{R} = \mathbf{C}\mathbf{C}^{\mathrm{H}} + \mathbf{S}\mathbf{S}^{\mathrm{H}} = \sum_{k=1}^{K}\mathbf{c}_k\mathbf{c}_k^{\mathrm{H}} + \mathbf{S}\mathbf{S}^{\mathrm{H}} = \sum_{k=1}^{K}\mathbf{C}_k + \mathbf{S}\mathbf{S}^{\mathrm{H}}, \quad (2)$$

where we have introduced the rank-1 matrix $\mathbf{C}_k = \mathbf{c}_k\mathbf{c}_k^{\mathrm{H}}$.

B. RIS Model

We model the RIS as a collection of discrete passive phase shifters, which can be individually controlled from the DFBS via a low-rate control link. Specifically, we assume that the RIS comprises N elements and model its spatial response as that of a uniform rectangular array (URA). The phase shifts of the RIS are collected in the vector $\boldsymbol{\omega}_t = [\omega_{t,1}, \ldots, \omega_{t,N}]^{\mathrm{T}} \in \Omega^N$, where $\omega_{t,i}$ denotes the phase shift introduced by the ith RIS element. Here, $t \in \{\mathrm{c}, \mathrm{r}\}$ with c and r denoting comm-RIS and radar-RIS, respectively.

C. Communication and Radar Channel Model

Let $\mathbf{H}_{\mathrm{br}} \in \mathbb{C}^{N\times M}$ denote the MIMO channel matrix for the DFBS-comm-RIS link. Let $\mathbf{h}_{\mathrm{bu},k}^{\mathrm{H}} \in \mathbb{C}^{1\times M}$ and $\mathbf{h}_{\mathrm{ru},k}^{\mathrm{H}} \in \mathbb{C}^{1\times N}$ denote the multiple input single output (MISO) channel vectors of the kth UE corresponding to the DFBS-UE and RIS-UE links, respectively. The overall channel vector $\mathbf{h}_k^{\mathrm{H}}$ comprising of the direct link and the additional link via the RIS is given by

$$\begin{aligned}\mathbf{h}_k^{\mathrm{H}} &= \mathbf{h}_{\mathrm{bu},k}^{\mathrm{H}} + \mathbf{h}_{\mathrm{ru},k}^{\mathrm{H}}\mathrm{diag}(\boldsymbol{\omega}_{\mathrm{c}})\mathbf{H}_{\mathrm{br}} \\ &= \mathbf{h}_{\mathrm{bu},k}^{\mathrm{H}} + \boldsymbol{\omega}_{\mathrm{c}}^{\mathrm{T}}\mathrm{diag}(\mathbf{h}_{\mathrm{ru},k}^{\mathrm{H}})\mathbf{H}_{\mathrm{br}} \in \mathbb{C}^{1\times M}. \end{aligned} \quad (3)$$

The signal received at the kth UE is then

$$y_k = \mathbf{h}_k^{\mathrm{H}}\mathbf{x}_n + n_k = \mathbf{h}_k^{\mathrm{H}}\left(\mathbf{C}\mathbf{d}_n + \mathbf{S}\mathbf{w}_n\right) + n_k, \quad (4)$$

where n_k is the additive Gaussian receiver noise having zero mean and variance σ^2.

For the radar channel model, let θ_j denote the angular location of the jth target with respect to (w.r.t.) the DFBS. Then the DFBS-target channel for the jth target is modeled as an LoS channel and is given by

$$\mathbf{g}_{\mathrm{bt},j}^{\mathrm{H}} = \alpha_{\mathrm{bt,j}}\mathbf{a}^{\mathrm{H}}(\theta_j) \in \mathbb{C}^{1\times M}, \quad (5)$$

where $\alpha_{\mathrm{bt,j}}$ is the complex path gain and $\mathbf{a}(\cdot)$ is the array response vector of the DFBS. We denote the channel from the radar-RIS to the jth target by $\mathbf{g}_{\mathrm{rt},j}^{\mathrm{H}} \in \mathbb{C}^{1\times N}$. The overall channel between the DFBS and the jth target is then

$$\begin{aligned}\mathbf{g}_j^{\mathrm{H}} &= \mathbf{g}_{\mathrm{bt},j}^{\mathrm{H}} + \mathbf{g}_{\mathrm{rt},j}^{\mathrm{H}}\mathrm{diag}(\boldsymbol{\omega}_{\mathrm{r}})\mathbf{G}_{\mathrm{br}} \\ &= \mathbf{g}_{\mathrm{bt},j}^{\mathrm{H}} + \boldsymbol{\omega}_{\mathrm{r}}^{\mathrm{T}}\mathrm{diag}(\mathbf{g}_{\mathrm{rt},j}^{\mathrm{H}})\mathbf{G}_{\mathrm{br}} \in \mathbb{C}^{1\times M}, \end{aligned} \quad (6)$$

where $\mathbf{G}_{\mathrm{br}} \in \mathbb{C}^{N\times M}$ is the channel between the DFBS and radar-RIS. Whenever the radar-RIS is not used or available, we simply set $\boldsymbol{\omega}_{\mathrm{r}}$ to zero.

In this paper, we assume that all the wireless channels are perfectly known at the BS. In practice, we need to estimate the associated channels $\mathbf{h}_k^{\mathrm{H}}$ and $\mathbf{g}_j^{\mathrm{H}}$, including cascaded channels $\mathrm{diag}(\mathbf{h}_{\mathrm{ru},k}^{\mathrm{H}})\mathbf{H}_{\mathrm{br}}$ and $\mathrm{diag}(\mathbf{g}_{\mathrm{rt},j}^{\mathrm{H}})\mathbf{G}_{\mathrm{br}}$. The cascaded channels involving the RIS for communication (sensing) may be estimated from uplink pilots (respectively, the target echo signals) at the DFBS using channel estimation techniques discussed in [36].

III. Problem Formulation

The performance of an ISAC system is characterized by the communication and radar sensing metrics, which are used to design the transmit beamformers and the RIS reflection patterns.

A. Communications Metric

The quality of service for a multi-user MIMO communication system in terms of the spectral efficiency or rate of the UEs is determined by the SINR at each UE. To ensure a minimum SINR for all the UEs, we consider the worst-case SINR or the so-called fairness SINR as the communication metric.

To arrive at an expression for the SINR, let us express the received signal at the kth UE, i.e., (4) as

$$y_k = \mathbf{h}_k^{\mathrm{H}} \left(\mathbf{c}_k d_k[n] + \sum_{j=1, j\neq k}^{K} \mathbf{c}_j d_j[n] + \sum_{m=1}^{M} \mathbf{s}_m w_m[n] \right) + n_k,$$

where the first term corresponds to the intended symbol received at the kth UE, the second term corresponds to the interference arising from the communication symbols intended for other UEs, and the third term corresponds to the interference arising from radar waveforms. Thus, the SINR for the kth UE is a function of $\boldsymbol{\omega}_c$ (through $\mathbf{h}_k$), $\mathbf{C}, \mathbf{S}$ and is given by

$$\begin{aligned}\gamma_k(\boldsymbol{\omega}_c, \mathbf{C}, \mathbf{S}) &= \frac{|\mathbf{h}_k^{\mathrm{H}} \mathbf{c}_k|^2}{\sum_{j=1, j\neq k}^{K} |\mathbf{h}_k^{\mathrm{H}} \mathbf{c}_j|^2 + \sum_{m=1}^{M} |\mathbf{h}_k^{\mathrm{H}} \mathbf{s}_m|^2 + \sigma^2} \\ &= \frac{\mathbf{h}_k^{\mathrm{H}} \mathbf{c}_k \mathbf{c}_k^{\mathrm{H}} \mathbf{h}_k}{\mathbf{h}_k^{\mathrm{H}} \left(\sum_{j=1, j\neq k}^{K} \mathbf{c}_j \mathbf{c}_j^{\mathrm{H}} + \mathbf{S}\mathbf{S}^{\mathrm{H}} \right) \mathbf{h}_k + \sigma^2} \\ &= \frac{\mathbf{h}_k^{\mathrm{H}} \mathbf{C}_k \mathbf{h}_k}{\mathbf{h}_k^{\mathrm{H}} \left(\mathbf{R} - \mathbf{C}_k \right) \mathbf{h}_k + \sigma^2} \end{aligned} \tag{7}$$

with the worst-case SINR being

$$\gamma_{\min} = \min_k \quad \gamma_k(\boldsymbol{\omega}_c, \mathbf{C}, \mathbf{S}). \tag{8}$$

An alternative communication performance metric is the sum-rate of the users. While sum-rate enforces the overall network throughput, it does not ensure fairness among users. Hence, we adopt worst-case SINR as the communication performance metric.

B. Radar Sensing Metrics

Next, we describe sensing performance metrics that we use for the two scenarios: when we do not use the radar-RIS and when we use the radar-RIS.

1) Beampattern Matching and Cross-Correlation Error: A MIMO radar system detects and tracks targets by transmitting signals in certain desired directions. This is achieved by designing multiple beams that match a desired beampattern while keeping the correlation between different beams as small as possible [12], [15].

To ensure that sufficient power reaches different target locations, we need to choose a desired pattern $d(\theta)$ that has main beams pointing in the direction of different targets. Furthermore, the comm-RIS is useful only if sufficient power reaches the comm-RIS in the first place. Thus, the desired pattern should also form a beam towards the direction of the comm-RIS from the DFBS. Denoting the direction of the comm-RIS from the DFBS as ζ_{r}, the desired pattern is chosen to be a superposition of multiple rectangular beams of width ϵ degrees with centers around $\{\theta_k\}_{k=1}^{T}$ and ζ_{r} as

$$d(\theta) = \begin{cases} 1, & \text{if} \quad \theta \in [\theta_k - \epsilon, \theta_k + \epsilon], \\ 1, & \text{if} \quad \theta \in [\zeta_{\mathrm{r}} - \epsilon, \zeta_{\mathrm{r}} + \epsilon], \\ 0, & \text{elsewhere.} \end{cases} \tag{9}$$

The power radiated from the DFBS towards the direction θ is given by

$$J(\theta) = \mathbb{E}\left[|\mathbf{a}^{\mathrm{H}}(\theta) \mathbf{x}_n|^2 \right] = \mathbf{a}^{\mathrm{H}}(\theta) \mathbf{R} \mathbf{a}(\theta). \tag{10}$$

For a desired beampattern $d(\theta)$, the beampattern mismatch error evaluated over a discrete grid of L angles $\{\tilde{\theta}_i\}_{i=1}^{L}$ is a function of $\mathbf{R}$ and is given by

$$L_1(\mathbf{R}, \tau) = \frac{1}{L} \sum_{\ell=1}^{L} |J(\tilde{\theta}_\ell) - \tau d(\tilde{\theta}_\ell)|^2, \tag{11}$$

where τ is the unknown autoscale parameter. The cross-correlation of the signals reflected back by the targets at directions θ_i and θ_j is given by

$$J_c(\mathbf{R}, \theta_i, \theta_j) = \mathbb{E}\left[(\mathbf{a}^{\mathrm{H}}(\theta_i) \mathbf{x}_n)(\mathbf{x}_n^{\mathrm{H}} \mathbf{a}(\theta_j)) \right] = \mathbf{a}^{\mathrm{H}}(\theta_i) \mathbf{R} \mathbf{a}(\theta_j),$$

with the average squared cross-correlation being

$$L_2(\mathbf{R}) = \frac{2}{T^2 - T} \sum_{i=1}^{T-1} \sum_{j=i+1}^{T} |J_c(\mathbf{R}, \theta_i, \theta_j)|^2. \tag{12}$$

We design radar beams that minimize a weighted sum of beampattern mismatch error and the average squared cross-correlation [15]

$$L(\mathbf{R}, \tau) = w_b L_1(\mathbf{R}, \tau) + w_c L_2(\mathbf{R}), \tag{13}$$

where w_b and w_c are the known weights that determine the relative importance of the two terms.

2) Worst-Case Target Illumination Power: Whenever the direct paths between the DFBS and the targets are weak or blocked, forming multiple beams at the DFBS towards different targets by adopting a beampattern mismatch criterion will not be useful as the target illumination power will be very small. To enable sensing in such scenarios, radar-RIS can be used. However, due to the fully passive nature of the RIS, obtaining cross-correlation optimal beams directed towards targets is not possible. Therefore, we adopt an alternative metric and propose to maximize the worst-case target illumination power to design the sensing beamformers.

The power of the signal received at the mth target corresponding to the transmitted waveform $\mathbf{x}_n$ is $\mathbb{E}\left[|\mathbf{g}_m^{\mathrm{H}} \mathbf{x}_n|^2 \right]$. The worst-case target illumination power is given by

$$\begin{aligned} Q(\mathbf{R}, \boldsymbol{\omega}_{\mathrm{r}}) &= \min_m \quad \mathbb{E}\left[|\mathbf{g}_m^{\mathrm{H}} \mathbf{x}_n|^2 \right] \\ &= \min_m \quad \mathbf{g}_m^{\mathrm{H}} \mathbf{R} \mathbf{g}_m = \min_m \quad \mathrm{Tr}\left(\mathbf{R} \mathbf{D}_m \right), \end{aligned} \tag{14}$$

where $\mathbf{D}_m = \mathbf{g}_m \mathbf{g}_m^{\mathrm{H}}$ and Q depends on $\boldsymbol{\omega}_{\mathrm{r}}$ through $\{\mathbf{g}_m, m = 1, \ldots, M\}$ [c.f. (6)].

Instead of Q, one may design the system to improve the received SINR of the radar echoes, a metric that directly impacts the target detection and estimation performance. However, the radar SINR not only depends on the transmit beamforming but also on the receiver radar processing adopted at the DFBS. Since our focus is on the transmit beamforming and RIS phase shift design, we restrict to the metrics in (13) and (14).

C. Design Problems

We now introduce the problems of designing the transmit beamformers at the DFBS and the RIS phase shifts for the two settings. For the setting [cf. Fig. 1(a)] with the comm-RIS assisting DFBS in communicating with multiple

TABLE I
COMMUNICATION AND SENSING PERFORMANCE METRICS CONSIDERED IN THE PAPER

Scenario	Sensing metric	Communication metric
($\mathcal{P}1$): comm RIS-assisted system	Weighted sum of beampattern mismatch error and cross-correlation	Worst-case SINR
($\mathcal{P}2$): dual RIS-assisted system	Worst-case target illumination power	Worst-case SINR

users, we design the transmit beamformers $(\mathbf{C}, \mathbf{S})$ and the comm-RIS phase shifts $\boldsymbol{\omega}_{\rm c}$ by minimizing the sensing cost function (13) while ensuring a minimum SINR for all users. For the setting [cf. Fig. 1(b)], we propose to design the transmit beamformers $(\mathbf{C}, \mathbf{S})$ and the radar- and comm-RIS phase shifts $\boldsymbol{\omega}_{\rm c}$ and $\boldsymbol{\omega}_{\rm r}$, to maximize the worst-case target illumination power $Q(\mathbf{R}, \boldsymbol{\omega}_{\rm r})$ [cf. (14)] while ensuring a minimum SINR for all the users. We formulate the design problem in the first setting as

$$\begin{aligned}
&\underset{\mathbf{S},\mathbf{C},\tau,\boldsymbol{\omega}_{\rm c}}{\text{minimize}}\ L(\mathbf{R},\tau)\\
(\mathcal{P}1):\ &\text{subject to } \mathbf{R}=\mathbf{C}\mathbf{C}^{\rm H}+\mathbf{S}\mathbf{S}^{\rm H}\ \in \mathbb{S}_+^M && \text{(15a)}\\
&\qquad [\mathbf{R}]_{i,i}=P_t/M,\quad i=1,\ldots,M && \text{(15b)}\\
&\qquad \gamma_k(\boldsymbol{\omega}_{\rm c},\mathbf{C},\mathbf{S})\geq\Gamma,\ k=1,\ldots,K && \text{(15c)}\\
&\qquad \boldsymbol{\omega}_{\rm c}\in\Omega^N, && \text{(15d)}
\end{aligned}$$

and in the second setting as

$$\begin{aligned}
&\underset{\mathbf{C},\mathbf{S},\boldsymbol{\omega}_{\rm c},\boldsymbol{\omega}_{\rm r}}{\text{maximize}}\ Q(\mathbf{R},\boldsymbol{\omega}_{\rm r})\\
(\mathcal{P}2):\ &\text{subject to } \mathbf{R}=\mathbf{C}\mathbf{C}^{\rm H}+\mathbf{S}\mathbf{S}^{\rm H}\ \in \mathbb{S}_+^M && \text{(16a)}\\
&\qquad [\mathbf{R}]_{i,i}=P_t/M,\quad i=1,\ldots,M && \text{(16b)}\\
&\qquad \gamma_k(\boldsymbol{\omega}_{\rm c},\mathbf{C},\mathbf{S})\geq\Gamma,\quad k=1,\ldots,K && \text{(16c)}\\
&\qquad \boldsymbol{\omega}_{\rm c}\in\Omega^N,\ \boldsymbol{\omega}_{\rm r}\in\Omega^N. && \text{(16d)}
\end{aligned}$$

Here, P_t is the total transmit power with (15b) and (16b) denoting the power constraint per antenna element, Γ is the SINR requirement of each user, and recall that τ is the autoscale parameter. The constraints (15d) and (16d) are due to the fact that the RIS is fully passive and can only reflect (i.e., phase shift) the incident signal to different directions. The optimization problem (15) is non-convex because of the quadratic equality in (15a), fractional term in (15c), and unit-modulus constraint in (15d).

In contrast to $(\mathcal{P}1)$, we use a different objective function in $(\mathcal{P}2)$. In addition to the design of the transmit beamformers and comm-RIS phase shifts, we also design the radar-RIS phase shifts in $(\mathcal{P}2)$. Optimization problem $(\mathcal{P}2)$ is also non-convex because of the quadratic equality (16a), fractional term in the constraint (16c), and unit-modulus constraints (16d). We summarize the details of performance metrics considered for the two scenarios in Table I.

IV. PROPOSED ALTERNATING OPTIMIZATION SOLVER

In this section, we develop solvers for $(\mathcal{P}1)$ and $(\mathcal{P}2)$ based on alternating optimization.

A. Proposed Solver for ($\mathcal{P}1$)

Problem $(\mathcal{P}1)$ to design $\mathbf{C}$, $\mathbf{S}$, and $\boldsymbol{\omega}_{\rm c}$ is not convex in the variables. Therefore, we propose to solve the optimization problem by alternatingly optimizing the beamformers and the autoscale parameter (i.e., $\mathbf{C}, \mathbf{S}, \tau$) while keeping the phase shifts (i.e., $\boldsymbol{\omega}_{\rm c}$) fixed, and vice versa. Specifically, in the first subproblem, we fix the comm-RIS phase shifts and design the beamformers to minimize the beampattern mismatch error while ensuring a minimum SINR for the users. Next, keeping the beamformers fixed, we optimize the comm-RIS phase shifts to maximize the worst-case SINR for all the UEs. We repeat the aforementioned steps till convergence.

1) Updating $\mathbf{C}$, $\mathbf{S}$, and τ, Given $\boldsymbol{\omega}_{\rm c}$: Let us now consider the subproblem of designing the beamformers $\mathbf{C}$ and $\mathbf{S}$ by fixing the comm-RIS phase shifts $\boldsymbol{\omega}_{\rm c}$ for an appropriately selected SINR threshold Γ. That is, we solve [12]:

$$\begin{aligned}
&\underset{\mathbf{S},\mathbf{C},\tau}{\text{minimize}}\ L(\mathbf{R},\tau)\\
&\text{subject to } \mathbf{R}=\mathbf{C}\mathbf{C}^{\rm H}+\mathbf{S}\mathbf{S}^{\rm H}\ \in \mathbb{S}_+^M\\
&\qquad [\mathbf{R}]_{i,i}=P_t/M,\quad i=1,\ldots,M\\
&\qquad \gamma_k(\mathbf{R})\geq\Gamma,\quad k=1,\ldots,K, && \text{(17)}
\end{aligned}$$

which is still a non-convex problem. To solve (17), we use the procedure from [12], which is provided here for self containment. From (2) and (7), the SINR constraints may be expressed as

$$\left(1+\Gamma^{-1}\right)\mathbf{h}_k^{\rm H}\mathbf{C}_k\mathbf{h}_k\geq\mathbf{h}_k^{\rm H}\mathbf{R}\mathbf{h}_k+\sigma^2 \qquad (18)$$

for $k=1,\ldots,K$. Thus, the subproblem (17) can be equivalently written as

$$\begin{aligned}
&\underset{\mathbf{R},\mathbf{C}_1,\ldots,\mathbf{C}_K,\mathbf{S},\tau}{\text{minimize}}\ L(\mathbf{R},\tau)\\
&\text{subject to } \mathbf{R}=\sum_{k=1}^K\mathbf{C}_k+\mathbf{S}\mathbf{S}^{\rm H},\\
&\qquad \mathbf{R}-\sum_{k=1}^K\mathbf{C}_k\ \in\mathbb{S}_+^M,\quad \mathbf{R}\in\mathbb{S}_+^M, && \text{(19)}\\
&\qquad \left(1+\Gamma^{-1}\right)\mathbf{h}_k^{\rm H}\mathbf{C}_k\mathbf{h}_k\geq\mathbf{h}_k^{\rm H}\mathbf{R}\mathbf{h}_k+\sigma^2,\\
&\qquad \operatorname{rank}(\mathbf{C}_k)=1,\quad k=1,\ldots,K,\\
&\qquad [\mathbf{R}]_{i,i}=P_t/M,\quad i=1,\ldots,M.
\end{aligned}$$

By dropping the quadratic equality constraint and replacing the unit-rank constraint with a weaker semidefinite constraint, we obtain the following relaxed convex optimization problem

$$\begin{aligned}
&\underset{\mathbf{R},\mathbf{C}_1,\ldots,\mathbf{C}_K,\tau}{\text{minimize}}\ L(\mathbf{R},\tau)\\
&\text{subject to } \mathbf{R}\in\mathbb{S}_+^M,\quad \mathbf{R}-\sum_{k=1}^K\mathbf{C}_k\in\mathbb{S}_+^M\\
&\qquad [\mathbf{R}]_{i,i}=P_t/M,\quad i=1,2,\ldots,M && \text{(20)}\\
&\qquad \left(1+\Gamma^{-1}\right)\mathbf{h}_k^{\rm H}\mathbf{C}_k\mathbf{h}_k\geq\mathbf{h}_k^{\rm H}\mathbf{R}\mathbf{h}_k+\sigma^2,\\
&\qquad \mathbf{C}_k\in\mathbb{S}_+^M,\quad k=1,\ldots,K,
\end{aligned}$$

which is a semidefinite quadratic program (SQP) that can be efficiently solved using off-the-shelf solvers. Let us denote the solution of (20) by $\hat{\mathbf{R}}, \tilde{\mathbf{C}}_1, \ldots, \tilde{\mathbf{C}}_K$. In general, Gaussian randomization is used to extract the unit-rank solution. Interestingly, for (20), the required precoders can be computed in closed form as in the next theorem [12, Theo. 1]:

Theorem 1: The communication beamformers $\hat{\mathbf{C}} = [\hat{\mathbf{c}}_1, \ldots, \hat{\mathbf{c}}_K] \in \mathbb{C}^{M\times K}$ *can be computed as*

$$\hat{\mathbf{c}}_k = \frac{\tilde{\mathbf{C}}_k \mathbf{h}_k}{\sqrt{\mathbf{h}_k^{\mathrm{H}} \tilde{\mathbf{C}}_k \mathbf{h}_k}}, \quad \hat{\mathbf{C}}_k = \hat{\mathbf{c}}_k \hat{\mathbf{c}}_k^{\mathrm{H}}, \quad k = 1, \ldots, K. \tag{21}$$

Furthermore, the radar beamformers $\hat{\mathbf{S}} = [\hat{\mathbf{s}}_1, \ldots, \hat{\mathbf{s}}_M] \in \mathbb{C}^{M\times M}$ *can be obtained using the Cholesky decomposition as*

$$\hat{\mathbf{R}} - \sum_{k=1}^{K} \hat{\mathbf{C}}_k := \hat{\mathbf{S}}\hat{\mathbf{S}}^{\mathrm{H}}. \tag{22}$$

Proof: We show that the solution given by (21) and (22) is indeed an optimal solution to (20). By construction, $\hat{\mathbf{C}}_k$ satisfies the SINR constraints as $\mathbf{h}_k^{\mathrm{H}} \hat{\mathbf{C}}_k \mathbf{h}_k = \mathbf{h}_k^{\mathrm{H}} \tilde{\mathbf{C}}_k \mathbf{h}_k$. Since $\hat{\mathbf{R}} - \sum_{k=1}^{K} \tilde{\mathbf{C}}_k \in \mathbb{S}_+^M$ and $\mathbf{z}^{\mathrm{H}}(\tilde{\mathbf{C}}_k - \hat{\mathbf{C}}_k)\mathbf{z} = \mathbf{z}^{\mathrm{H}}\tilde{\mathbf{C}}_k\mathbf{z} - (\mathbf{h}_k^{\mathrm{H}}\tilde{\mathbf{C}}_k\mathbf{h}_k)^{-1}|\mathbf{z}^{\mathrm{H}}\tilde{\mathbf{C}}_k\mathbf{h}_k|^2 \geq 0$ for any $\mathbf{z}$ due to the Cauchy-Schwartz inequality, we have $\hat{\mathbf{R}} - \sum_{k=1}^{K} \tilde{\mathbf{C}}_k + \sum_{k=1}^{K}(\tilde{\mathbf{C}}_k - \hat{\mathbf{C}}_k) = \hat{\mathbf{R}} - \sum_{k=1}^{K} \hat{\mathbf{C}}_k \in \mathbb{S}_+^M$. Thus, $\hat{\mathbf{C}}_k, k = 1, 2, \ldots, K$ also form a feasible solution to (20). Further, since $\sum_{k=1}^{K} \hat{\mathbf{C}}_k + \hat{\mathbf{S}}\hat{\mathbf{S}}^{\mathrm{H}} = \hat{\mathbf{R}}$, the constructed solution does not change the objective value (which depends only on $\mathbf{R}$ and τ), and thus will yield the smallest objective value for (20). Therefore, the solution obtained using (21) and (22) is an optimal solution to (20). ∎

2) Updating $\boldsymbol{\omega}_{\mathrm{c}}$*, Given* $\mathbf{C}$*,* $\mathbf{S}$*, and* τ*:* The subproblem of finding the comm-RIS phase shifts, given $\mathbf{C}$, $\mathbf{S}$, and τ, simplifies to the feasibility problem

$$\begin{aligned} &\text{find } \boldsymbol{\omega}_{\mathrm{c}} \\ &\text{subject to } \gamma_k(\boldsymbol{\omega}_{\mathrm{c}}) \geq \Gamma, \quad k = 1, \ldots, K \\ &\qquad \boldsymbol{\omega}_{\mathrm{c}} \in \Omega^N. \end{aligned} \tag{23}$$

However, the fixed choice of $\boldsymbol{\omega}_{\mathrm{c}}$ in (17) is already a solution to the above problem. Since different choices of $\boldsymbol{\omega}_{\mathrm{c}}$ lead to different achievable SINRs at the UEs, i.e., better Γ, we can alternatively design $\boldsymbol{\omega}_{\mathrm{c}}$ to improve the achievable SINR at the UEs by solving

$$\Gamma_1 = \underset{\boldsymbol{\omega}_{\mathrm{c}} \in \Omega^N}{\text{maximize}} \quad \min_{1\leq k\leq K} \gamma_k(\boldsymbol{\omega}_{\mathrm{c}}) \tag{24}$$

where $\Gamma_1 \geq \Gamma$. Due to the unit modulus constraint and the fractional cost function, (24) is a non-convex optimization problem in $\boldsymbol{\omega}_{\mathrm{c}}$ and its exact solution is difficult to compute.

To solve (24), we first express it as a generalized linear fractional program with multiple ratios by expressing the SINR explicitly in terms of $\boldsymbol{\omega}_{\mathrm{c}}$. Let us define the vectors $\mathbf{a}_{k,m} = [(\mathrm{diag}(\mathbf{h}_{\mathrm{ru},k}^{\mathrm{H}})\mathbf{H}_{\mathrm{br}}\mathbf{c}_m)^{\mathrm{T}}, \mathbf{h}_{\mathrm{bu},k}^{\mathrm{H}}\mathbf{c}_m]^{\mathrm{T}}$ and $\mathbf{b}_{k,m} = [(\mathrm{diag}(\mathbf{h}_{\mathrm{ru},k}^{\mathrm{H}})\mathbf{H}_{\mathrm{br}}\mathbf{s}_m)^{\mathrm{T}}, \mathbf{h}_{\mathrm{bu},k}^{\mathrm{H}}\mathbf{s}_m]^{\mathrm{T}}$ each of length $N+1$. Let us also define the square matrices $\mathbf{A}_k = \mathbf{a}_{k,k}\mathbf{a}_{k,k}^{\mathrm{H}}$ and $\mathbf{B}_k = \sum_{j=1,j\neq k}^{K} \mathbf{a}_{k,j}\mathbf{a}_{k,j}^{\mathrm{H}} + \sum_{m=1}^{M} \mathbf{b}_{k,m}\mathbf{b}_{k,m}^{\mathrm{H}}$ of size $N+1$. From (3), we can then express SINR in (7) as

$$\gamma_k(\mathbf{w}) = \frac{\mathbf{w}^{\mathrm{H}}\mathbf{A}_k\mathbf{w}}{\mathbf{w}^{\mathrm{H}}\mathbf{B}_k\mathbf{w} + \sigma^2} = \frac{\mathrm{Tr}\,(\mathbf{A}_k\mathbf{w}\mathbf{w}^{\mathrm{H}})}{\mathrm{Tr}\,(\mathbf{B}_k\mathbf{w}\mathbf{w}^{\mathrm{H}}) + \sigma^2} \tag{25}$$

where $\mathbf{w}^{\mathrm{H}} = [\boldsymbol{\omega}_{\mathrm{c}}^{\mathrm{T}}, 1]$. By letting $\mathbf{W} = \mathbf{w}\mathbf{w}^{\mathrm{H}}$, we rewrite (24) as

$$\begin{aligned} \Gamma_2 = \underset{\mathbf{W}\in\mathbb{S}_+^{N+1}}{\text{maximize}} \ & \min_{1\leq k\leq K} \frac{\mathrm{Tr}\,(\mathbf{A}_k\mathbf{W})}{\mathrm{Tr}\,(\mathbf{B}_k\mathbf{W}) + \sigma^2} \\ \text{subject to } & [\mathbf{W}]_{ii} = 1, \quad i = 1, \ldots, N+1, \end{aligned} \tag{26}$$

where we have introduced a less restrictive and convex semidefinite constraint on $\mathbf{W}$ instead of the rank one constraint. The problem in (26) is a generalized linear fractional program with a convex constraint set. Next, we develop an iterative procedure to solve (26) using the generalized Dinkelbach-type method [37], which is guaranteed to converge to the solution of (26).

Let us denote the iterate at step t as $\mathbf{W}^{(t)}$. We first compute an estimate of $\gamma_{\min}$ as

$$\lambda^{(t)} = \min_{1\leq k\leq K} \frac{\mathrm{Tr}\left(\mathbf{A}_k\mathbf{W}^{(t-1)}\right)}{\mathrm{Tr}\left(\mathbf{B}_k\mathbf{W}^{(t-1)}\right) + \sigma^2}. \tag{27}$$

Next, we update $\mathbf{W}^{(t)}$ as

$$\begin{aligned} \mathbf{W}^{(t)} = \underset{\mathbf{W}\in\mathbb{S}_+^{N+1}}{\mathrm{argmax}} \ & \min_{1\leq k\leq K} \mathrm{Tr}\,(\mathbf{A}_k\mathbf{W}) - \lambda^{(t)}\left(\mathrm{Tr}\,(\mathbf{B}_k\mathbf{W}) + \sigma^2\right) \\ \text{subject to } & [\mathbf{W}]_{ii} = 1, \quad i = 1, \ldots, N+1, \end{aligned} \tag{28}$$

where $\lambda^{(t)} \geq \Gamma_1$ and $\min_k\{\mathrm{Tr}(\mathbf{A}_k\mathbf{W}^{(t)}) - \lambda^{(t)}(\mathrm{Tr}(\mathbf{B}_k\mathbf{W}^{(t)}) + \sigma^2)\} = 0$ at optimality. This condition can be used to stop the iterations. In practice, we may update $\lambda^{(t)}$ and $\mathbf{W}^{(t)}$ till $\|\mathbf{W}^{(t)} - \mathbf{W}^{(t-1)}\| \leq \mathtt{Tol}$, where $\mathtt{Tol}$ is the tolerance value.

Let us denote the solution from this iterative procedure as $\tilde{\mathbf{W}}$. To recover a rank-1 solution from $\tilde{\mathbf{W}}$, we use Gaussian randomization [38]. That is, we generate N_{rand} realization of complex Gaussian random vectors $\tilde{\mathbf{w}}_i, i = 1, \cdots, N_{\mathrm{rand}}$ with zero mean and covariance matrix $\tilde{\mathbf{W}}$. We then normalize $\tilde{\mathbf{w}}_i$ to obtain unit modulus vectors $\hat{\mathbf{w}}_i$ with entries

$$[\hat{\mathbf{w}}_i]_n = \begin{cases} [\tilde{\mathbf{w}}_i]_m/|[\tilde{\mathbf{w}}_i]_m|, & \text{for } m = 1, 2, \ldots, N, \\ 1, & \text{otherwise.} \end{cases}$$

We choose the realization that results in the largest worst-case SINR as

$$i^\star = \underset{1\leq i\leq N_{\mathrm{rand}}}{\arg\max} \quad \min_{1\leq k\leq K} \quad \gamma_k(\hat{\mathbf{w}}_i), \tag{29}$$

and the optimal comm-RIS phase shift as $[\hat{\boldsymbol{\omega}}_{\mathrm{c}}]_n = [\hat{\mathbf{w}}_{i^\star}^*]_n$ for $n = 1, \ldots, N$. The actual worst-case SINR corresponding to the rank-1 solution obtained from this Gaussian randomization $\Gamma_3 = \min_k\{\gamma_k(\hat{\mathbf{w}}_{i^\star}), k = 1, \cdots, K\}$ will be in the interval 0 and Γ_1. Alternatively, we can compute the required rank-1 solution by computing the dominant eigenvector of $\tilde{\mathbf{W}}$. However, there is no guarantee that such a solution satisfies the SINR constraints. On the other hand, in Gaussian randomization, we can draw multiple realizations of Gaussian random vectors with an advantage of repeating the procedure till a feasible solution is obtained. Hence, we adopt Gaussian randomization.

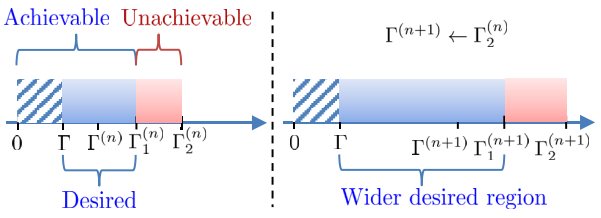

Fig. 2. Illustration of choosing Γ. The horizontal axis denotes the fairness SINR. Increasing the target SINR from $\Gamma^{(n)}$ to $\Gamma^{(n+1)} = \Gamma_2^{(n)}$ leads to a wider desired region width resulting in a higher probability of Gaussian randomization yielding a solution in the desired region.

3) Practical Considerations for Choosing Γ: Let us denote Γ_1, Γ_2, and Γ_3 at the nth iteration as $\Gamma_1^{(n)}$, $\Gamma_2^{(n)}$, and $\Gamma_3^{(n)}$, respectively. Since we have more degrees of freedom in choosing $\mathbf{W}$ in the relaxed problem (26) than with a unit modulus (or rank) constraint as in (24), we have $\Gamma_2^{(n)} \geq \Gamma_1^{(n)} \geq \Gamma$, in general. In other words, the achievable SINR is much higher if we ignore the passive nature of the RIS, but is not practically realizable. At each iteration, we can only evaluate $\Gamma_2^{(n)}$ and $\Gamma_3^{(n)}$, but we cannot compute $\Gamma_1^{(n)}$.

To design the beamformers and the comm-RIS phase shifts, starting from an initial comm-RIS phase shift, we update $\mathbf{C}$ and $\mathbf{S}$ using (21) and (22), respectively. Then, we update $\boldsymbol{\omega}_c$ as in (29). Specifically, in the nth iteration, we solve (20) with the desired SINR Γ set to $\Gamma^{(n)}$. We repeat the alternating optimization until $\Gamma_3^{(n)} \geq \Gamma$, where recall that $\Gamma_3^{(n)} \in [0, \Gamma_1^{(n)}]$ is the actual SINR after Gaussian randomization. We refer to the interval $[0, \Gamma_1^{(n)}]$ as the *achievable region*. The interval with values of SINR that are both achievable and desired, i.e., the interval between Γ and $\Gamma_1^{(n)}$ is referred to as the *desired region*. Whenever the width of the desired region is small, it is less likely that the Gaussian randomization procedure (described in the previous subsection) produces realization in the desired region. Therefore, it is possible to have $\Gamma_3^{(n)} < \Gamma$, thereby violating the communication SINR requirements. A narrow desired region, in other words, indicates that the RIS phase shifts alone cannot significantly improve the SINR of UEs. At the same time, a higher SINR is often achievable by designing beamformers since we have higher flexibility (i.e., without unit modulus and rank constraints). To circumvent this issue, in the $(n+1)$th iteration, we design the beamformers so as to achieve an SINR higher than $\Gamma^{(n)}$ by setting $\Gamma^{(n+1)} = \Gamma_2^{(n)}$, thereby increasing the width of the desired region. With a widened desired region, it is more likely that Gaussian randomization produces realization with $\Gamma_3^{(n+1)} \geq \Gamma$, as desired. This is illustrated in Fig. 2. The proposed procedure for solving $(\mathcal{P}1)$ is summarized as Algorithm 1.

4) Computational Complexity: For an ϵ-accurate solution, the worst-case complexity for computing the beamformers, given the RIS phase shifts is that of an SDP with $(K+1)$ constraints and is of the order of about $\mathcal{O}\left(K^{6.5}M^{6.5}\log(1/\epsilon)\right)$ [12]. For the subproblem of computing the RIS phase shifts, given the beamformers, we solve an SDP for I_{in} Dinkelbach iterations in the inner loop. Thus, the complexity involved in obtaining the RIS phase shifts given the beamformers is of the order of about $\mathcal{O}\left(I_{\text{in}}N^{6.5}\log(1/\epsilon)\right)$. Suppose I_{out} be the number of iterations in the outer loop of the proposed alternating optimization algorithm. Then, the overall complexity is about $\mathcal{O}\left(I_{\text{out}}\left(K^{6.5}M^{6.5}+I_{\text{in}}N^{6.5}\right)\log(1/\epsilon)\right)$.

Algorithm 1 Solver for $(\mathcal{P}1)$

Initialization: $\Gamma^{(n)} = \Gamma$, $\boldsymbol{\omega}_{\text{c}}^{(n)} = \boldsymbol{\omega}_{\text{c}}^{(0)}$

1: **for** $n = 1, 2, \cdots,$ `MaxIter` **do**
2: Solve (20) with SINR constraint Γ set to $\Gamma^{(n)}$ to update $\hat{\mathbf{R}}$ and $\{\tilde{\mathbf{C}}_1, \tilde{\mathbf{C}}_2, \cdots, \tilde{\mathbf{C}}_K\}$.
3: Update $\{\hat{\mathbf{C}}_1, \hat{\mathbf{C}}_2, \cdots, \hat{\mathbf{C}}_K\}$ using (21).
4: Update $\hat{\mathbf{S}}$ using (22).
5: Update $\boldsymbol{\omega}_{\text{c}}$ by updating $\mathbf{W}$ as in (29) and compute $\Gamma_3^{(n)}$.
6: **if** $\Gamma_3^{(n)} \geq \Gamma$ **then** `break`
7: Set $\Gamma^{(n)} = \Gamma_2^{(n)}$.

B. Proposed Solver for $(\mathcal{P}2)$

We next develop a solver to design the transmit beamformers and the phase shifts of both the radar-RIS and comm-RIS, i.e., we present a solver for Problem $(\mathcal{P}2)$. As before, we adopt an alternating optimization based procedure to solve the non-convex optimization problem $(\mathcal{P}2)$, wherein we design the beamformers while keeping the phase shifts fixed and vice versa.

1) Updating $\mathbf{C}$ and $\mathbf{S}$, Given $\boldsymbol{\omega}_{\text{c}}$ and $\boldsymbol{\omega}_{\text{r}}$: Given $\boldsymbol{\omega}_{\text{c}}$ and $\boldsymbol{\omega}_{\text{r}}$, $(\mathcal{P}2)$ simplifies to a problem with exactly the same constraints as (20), but with a different objective function, i.e., we have

$$\begin{aligned}
\underset{\mathbf{R},\mathbf{C}_1,\ldots,\mathbf{C}_K}{\text{maximize}} \ \min_{m} \quad & \text{Tr}\left(\mathbf{R}\mathbf{D}_m\right) \\
\text{subject to } \mathbf{R} \in \mathbb{S}_+^M, \quad & \mathbf{R} - \sum_{k=1}^{K} \mathbf{C}_k \in \mathbb{S}_+^M \\
& [\mathbf{R}]_{i,i} = P_t/M, \quad i = 1, 2, \ldots, M \\
& \left(1+\Gamma^{-1}\right)\mathbf{h}_k^{\text{H}}\mathbf{C}_k\mathbf{h}_k \geq \mathbf{h}_k^{\text{H}}\mathbf{R}\mathbf{h}_k + \sigma^2, \\
& \mathbf{C}_k \in \mathbb{S}_+^M, \quad k = 1, \ldots, K,
\end{aligned} \tag{30}$$

where we have replaced the SINR constraint in $(\mathcal{P}2)$ with an equivalent inequality in (18) and dropped the rank-one constraint on $\mathbf{C}_k$ as we did from (19) to (20). A rank-1 solution $\mathbf{C}_k$ and $\mathbf{S}$ is obtained using (21) and (22), respectively, after solving the above convex program. The constructed solution will yield the largest objective value for (30).

For a fixed $\mathbf{C}$ and $\mathbf{S}$, the subproblems of finding $\boldsymbol{\omega}_{\text{c}}$ and $\boldsymbol{\omega}_{\text{r}}$ are independent of each other and can be solved separately.

2) Updating $\boldsymbol{\omega}_{\text{c}}$, Given $\mathbf{C}$ and $\mathbf{S}$: The procedure for updating the comm-RIS phase shifts, given the beamformers $\mathbf{C}$ and $\mathbf{S}$ is exactly the same as the feasibility problem (23) for which we reuse the procedure described in Sections IV-A2 and IV-A3.

3) Updating $\boldsymbol{\omega}_{\text{r}}$, Given $\mathbf{C}$ and $\mathbf{S}$: We now discuss the design of radar-RIS phase shifts, where we maximize the worst-case target illumination power $Q(\mathbf{R}, \boldsymbol{\omega}_{\text{r}})$, given the beamformers $(\mathbf{C}, \mathbf{S})$.

Algorithm 2 Solver for $(\mathcal{P}2)$

Initialization: $\Gamma^{(n)} = \Gamma$, $\boldsymbol{\omega}_{\mathrm{c}}^{(n)} = \boldsymbol{\omega}_{\mathrm{c}}^{(0)}$, $\boldsymbol{\omega}_{\mathrm{r}}^{(n)} = \boldsymbol{\omega}_{\mathrm{r}}^{(0)}$

1: **for** $n = 1, 2, \cdots,$ `MaxIter` **do**
2: Solve (30) with SINR constraint Γ set to $\Gamma^{(n)}$ to update $\hat{\mathbf{R}}$ and $\{\hat{\mathbf{C}}_1, \hat{\mathbf{C}}_2, \cdots, \hat{\mathbf{C}}_K\}$.
3: Update $\{\hat{\mathbf{C}}_1, \hat{\mathbf{C}}_2, \cdots, \hat{\mathbf{C}}_K\}$ using (21).
4: Update $\hat{\mathbf{S}}$ using (22).
5: Update $\boldsymbol{\omega}_{\mathrm{c}}$ as in (29) and compute $\Gamma_3^{(n)}$.
6: Update $\boldsymbol{\omega}_{\mathrm{r}}$ via $\mathbf{U}$ by solving (31).
7: **if** $\Gamma_3^{(n)} \geq \Gamma$ **then** `break`
8: Set $\Gamma^{(n)} = \Gamma_2^{(n)}$.

From (6), we can express (14) explicitly in terms of $\boldsymbol{\omega}_{\mathrm{r}}$ as

$$Q(\mathbf{R}, \boldsymbol{\omega}_{\mathrm{r}}) = \min_{m} \quad \mathbf{u}^{\mathrm{H}} \mathbf{Q}_m \mathbf{u} = \min_{m} \quad \mathrm{Tr}\left(\mathbf{Q}_m \mathbf{U}\right)$$

where $\mathbf{U} = \mathbf{u}\mathbf{u}^{\mathrm{H}}$ with $\mathbf{u}^{\mathrm{H}} = [1, \boldsymbol{\omega}_{\mathrm{r}}^{\mathrm{T}}]$ and

$$\mathbf{Q}_m = \begin{bmatrix} \mathbf{g}_{\mathrm{bt},m}^{\mathrm{H}} \\ \mathrm{diag}\left(\mathbf{g}_{\mathrm{rt},m}^{*}\right) \mathbf{G}_{\mathrm{br}} \end{bmatrix} \mathbf{R} \left[\mathbf{g}_{\mathrm{bt},m} \quad \mathbf{G}_{\mathrm{br}}^{\mathrm{H}} \mathrm{diag}\left(\mathbf{g}_{\mathrm{rt},m}\right)\right].$$

To obtain the optimal phase shifts, we solve the following optimization problem:

$$\begin{aligned} \max_{\mathbf{U} \in \mathbb{S}_{+}^{N+1}} \quad & \min_{m} \quad \mathrm{Tr}\left(\mathbf{Q}_m \mathbf{U}\right) \\ \text{subject to } & [\mathbf{U}]_{i,i} = 1 \quad i = 1, \ldots, N+1, \end{aligned} \tag{31}$$

where we have dropped the non-convex rank constraint (i.e., $\mathrm{rank}\,(\mathbf{U}) = 1$) as before. The optimization problem (31) is convex and is then solved using off-the-shelf convex solvers. The required rank-1 solution is then obtained using Gaussian randomization (refer to Sec. IV-A2).

To ensure that sufficient power is radiated towards different target directions, we initialize radar-RIS phase shifts so that equally powerful beams are formed towards all target directions. The selection and update of the target SINR $\Gamma^{(n)}$ at each iteration is as before. The proposed procedure to solve $(\mathcal{P}2)$ is summarized as Algorithm 2.

4) Computational Complexity: Similar to the update of comm-RIS phase shifts, updation of radar-RIS phase shifts also involves solving an SDP with a complexity of $\mathcal{O}\left(N^{6.5}\log(1/\epsilon)\right)$. Hence, the overall complexity is about $\mathcal{O}\left(I_{\mathrm{out}} K^{6.5} M^{6.5} \log(1/\epsilon) + I_{\mathrm{out}}(I_{\mathrm{in}}+1) N^{6.5} \log(1/\epsilon)\right)$ flops, which is of the same order as that of Algorithm 1.

V. A Low-Complexity Alternative for $(\mathcal{P}1)$ and $(\mathcal{P}2)$

In the RIS phase shift design, an SDP is solved in each iteration of the Dinkelbach algorithm, which can be computationally expensive. In this section, we present an alternative, low-complexity approach, which we refer to as `Proposed-F`, to design ω_{c}. Let us recall that the original comm-RIS phase shift design problem is the feasibility problem given in (23). Instead of obtaining $\boldsymbol{\omega}_{\mathrm{c}}$ to maximize the worst-case SINR, an alternative sub-optimal approach is to solve the feasibility problem. We now show that the feasibility problem can also be solved using an SDP-based approach, but we solve only one SDP instead of I_{in} SDPs compared to Algorithm 1 and 2. Using (25), we can re-write the SINR constraint as

$$\mathrm{Tr}\left(\left(\mathbf{A}_k - \Gamma \mathbf{B}_k\right) \mathbf{W}\right) \geq \Gamma \sigma^2, \quad k = 1, \ldots, K,$$

where $\mathbf{W} = \mathbf{w}\mathbf{w}^{\mathrm{H}}$, and the feasibility problem (23) as

$$\begin{aligned} \text{find } & \mathbf{W} \\ \text{subject to } & \mathrm{Tr}\left(\left(\mathbf{A}_k - \Gamma \mathbf{B}_k\right) \mathbf{W}\right) \geq \Gamma \sigma^2, \quad k = 1, \ldots, K, \\ & [\mathbf{W}]_{i,i} = 1, \quad i = 1, \ldots, N+1, \\ & \mathrm{rank}\,(\mathbf{W}) = 1. \end{aligned}$$

On dropping the unit-rank constraint, we get an SDP. As before, the unit-rank solution can then be obtained using Gaussian randomization. As compared to the Dinkelbach approach, the feasibility check based approach only involves one SDP as opposed to I_{in} (typically 5-10 in practice) SDPs for the former. Hence, the overall computational complexity of the feasibility-based approach is $\mathcal{O}\left(N^{6.5}\log(1/\epsilon)\right)$.

To summarize, we first optimize the transmit precoders for the given comm-RIS phase shifts (say, $\boldsymbol{\omega}_{\mathrm{c}}^{(0)}$). Next, we update the comm-RIS phase shifts using the feasibility-based approach. With the feasibility-based approach, it is possible that $\min_k \gamma_k(\boldsymbol{\omega}_{\mathrm{c}}^{(1)}) < \min_k \gamma_k(\boldsymbol{\omega}_{\mathrm{c}}^{(0)})$. In such cases, we retain the previous value of the comm-RIS phase shifts and use $\boldsymbol{\omega}_{\mathrm{c}}^{(1)} = \boldsymbol{\omega}_{\mathrm{c}}^{(0)}$. Finally, we update the radar-RIS phase shifts.

TABLE II
Simulation Parameters

Parameter	Value
DFBS location	$(0, 0, 0)$ m
comm-RIS location	$(20, 13, 3)$ m
radar-RIS location	$(-6, 6, 3)$ m
Target angles w.r.t. DFBS	$(-70°, -50°, -30°, -20°, -10°)$
Target distance from DFBS	5 m

VI. Numerical Simulations

In this section, we present results from a number of numerical experiments to illustrate the benefits of RIS-enabled ISAC systems and performance of the proposed algorithms. Throughout the simulations, we model the DFBS as a ULA with $M = 16$ half-wavelength spaced elements. Both the comm- and radar-RISs are modeled as URAs comprising of quarter-wavelength spaced elements [17]. We model the entries of the channels $\mathbf{H}_{\mathrm{br}}$, $\mathbf{G}_{\mathrm{br}}$, and $\mathbf{h}_{\mathrm{ru},k}^{\mathrm{H}}$ for $k = 1, \ldots, K$ as Rician distributed random variables with a Rician factor of $\rho = 10$. The direct path for the UEs, i.e., $\mathbf{h}_{\mathrm{bu},k}^{\mathrm{H}}$ for $k = 1, \ldots, K$ is assumed to undergo Rayleigh fading. The remaining channels, namely, $\mathbf{g}_{\mathrm{bt},m}$ and $\mathbf{g}_{\mathrm{rt},m}$ for $m = 1, \ldots, T$ are modeled as LoS channels.

The receiver noise variance at the UEs is set to -94 dBm. The targets are assumed to be located in the far-field of both the DFBS and radar-RIS. User locations are drawn randomly from a rectangular grid having corners $(15, 8, 0)$ m, $(15, 18, 0)$ m, $(18, 8, 0)$ m, and $(18, 18, 0)$ m. The pathlosses of the radar-RIS and target links and DFBS and UE links are modeled as $30 + 25\log d$ dB and $30 + 36\log d$ dB, respectively. Pathlosses for the rest of the links are modeled

as $30 + 22 \log d$ dB with d m being the distance between concerned terminals. The remaining simulation parameters are summarized in Table II. Throughout this section, we use `Proposed-D` (from Section IV) and `Proposed-F` (From Section V) to refer to the proposed algorithms with Dinkelbach iterations and feasibility based approach, respectively, to design $\boldsymbol{\omega}_c$.

A. Comm-RIS Assisted ISAC System

We begin by presenting the designed transmit beampattern and the reflection profile of the comm-RIS. Then we present results from the Monte-Carlo experiments to show the benefits of RIS in ISAC systems in terms of the achievable SINR and worst-case illumination power at the target locations of interest by varying different system parameters such as SINR requirement (Γ), number of RIS elements (N), and number of users with direct path (K_d). In this section, we consider a two-target scenario, i.e., $T = 2$ with $\theta_1 = -50^\circ$ and $\theta_2 = -10^\circ$.

We compare the performance of the proposed methods in terms of transmit pattern, the fairness SINR (or min-rate), and the worst-case target illumination power with the following four schemes: (*i*) joint active and passive beamforming design (`JAPBD`) in [34], (*ii*) `RIS manual selection`, wherein we select the RIS phase profile to form equally powerful beams towards all the UEs, and (*iii*) `no RIS`, wherein we consider an ISAC system without RIS [12]. We compute the beamformers at the DFBS by solving (20) for both `RIS manual selection` and `no RIS` schemes. Although such manual selection of RIS phase shifts seem intuitive, they are agnostic to the task at hand and are not fairness SINR optimal. We also compare the proposed method with (*iv*) `sensing-only system`, which does not have any communication functionality or RIS [15]. For the `sensing-only system`, we solve ($\mathcal{P}1$) only w.r.t. $\mathbf{S}$ ($\mathbf{C}$ is set to zero) without the constraints (15c) and (15d). To simulate different schemes, we first run `JAPBD` to compute the minimum total transmit power required to achieve certain radar SNR, communication SINR, and average squared cross-correlation between the beams.[1] We then choose the resulting power as the total power constraint for the remaining schemes, thereby ensuring that all schemes utilize the same amount of transmit power.

1) Transmit Beampattern and RIS Reflection Pattern: For the ideal beampattern $d(\theta)$ in (9), we use a superposition of rectangular box functions of width $\epsilon = 10$ degrees. We set $w_b = w_c = 1$ in $L(\mathbf{R}, \tau)$ [cf. (13)]. To illustrate the beampattern obtained from Algorithm 1, we consider $K = 1$. We use $N = 100$ RIS elements and $\Gamma = 5$ dB. The transmit beampattern at the DFBS is shown in Figs. 3(a) and 3(b). The transmit pattern of a scheme that considers sum received SNR as the radar metric [34] results in a peak only towards one of the targets, resulting in the DFBS completely missing one of the targets. On the other hand, the transmit beampattern of the proposed algorithm has a response towards the two target locations of interest as well as towards the comm-RIS, as desired, thereby ensuring that none of the targets are missed.

[1]Our algorithm is independent of JAPBD. Since JAPBD is designed to meet the minimum required power, we simply use JAPBD to obtain a reference value for the power budget.

To gain further insights, we consider individual beampatterns of the radar and communication beamformers, where the radar beampattern is defined as $J_R(\theta) = \mathbf{a}^{\mathrm{H}}(\theta)\mathbf{S}\mathbf{S}^{\mathrm{H}}\mathbf{a}(\theta)$ and the beampattern related to the kth communication user is defined as $J_{C,k}(\theta) = \mathbf{a}^{\mathrm{H}}(\theta)\mathbf{c}_k\mathbf{c}_k^{\mathrm{H}}\mathbf{a}(\theta)$. To visualize the reflection pattern at RIS, we define the beampattern of RIS towards the direction cosine vector $\boldsymbol{\psi} \in \mathbb{R}^2$ for a signal incident on the RIS from the DFBS from the direction $\boldsymbol{\phi} \in \mathbb{R}^2$ as follows $J_{\mathrm{RIS}}(\boldsymbol{\psi}) = |\mathbf{r}^{\mathrm{H}}(\boldsymbol{\psi})\mathrm{diag}(\boldsymbol{\omega})\mathbf{r}(\boldsymbol{\phi})|$, where $\mathbf{r}(\cdot) \in \mathbb{C}^{N\times 1}$ is the array response vector of the RIS. The separate beampatterns (related to the sensing and communication beamformers) at the RIS is shown in Fig. 3(c). We observe that the radar beam has peaks towards target directions of interest and the communication beam has a stronger peak towards the RIS. Further, the radar beam has a dip in the direction of the RIS. This is desired since the comm-RIS is used solely to serve the UEs, and any amount of radar signals transmitted towards the UEs via the RIS could lead to potentially increased interference (hence lower SINR) at the communication UEs. While transmitting radar signals to communication UEs leads to interference, transmitting communication signals (known at the DFBS) to target locations actually helps in improving the target illumination power, and this explains the peaks of communication beams towards the targets. In Fig. 3(d), we show the reflection pattern of the RIS, where we can see that the RIS beampattern has a peak towards the user direction. This is intuitive since the RIS attempts to steer all the energy incident on it towards the single UE to maximize the received SINR. For larger values of K, unlike the $K = 1$ case, the reflection pattern at the RIS is often not interpretable as the SINR optimal design is not necessarily the pattern that forms beams towards $K > 1$ users.

In Fig. 4(a), we show convergence of the updates (27)-(28) that solve (26) for updating the comm-RIS phase shifts. Here, we use a particular channel realization with $K = 4$ (i.e., we have a fractional programming problem with four ratios). We observe that the updates converge in about 5 iterations. Next, in Fig. 4(b), we present the convergence of the overall alternating optimization algorithm. We observe that the worst-case target illumination power attains the maximum value in a few iterations. Moreover, the worst-case SINR also attains the desired value in a few iterations (not shown here). In general, we have observed that the proposed algorithm requires very few iterations for convergence. Hence, even though the sub-problem of the comm-RIS phase shift design is of higher complexity, the complexity of the overall algorithm is still not very high.

2) Monte-Carlo Simulations: We now consider a multi-user, multi-target scenario with $K = 4$, $T = 2$, and $N = 100$, unless mentioned otherwise. We present a number of results from Monte-Carlo experiments that are obtained by averaging over 100 independent realizations of the fading channel with different user locations. Unless mentioned otherwise, we use radar SNR requirement of 10 dB and a average squared cross-correlation of 10^{-5}.

In Fig. 5(a), we show the impact of the SINR constraint (Γ) on the fairness SINR of different methods. While the benchmark schemes provide exactly the minimum required SINR,

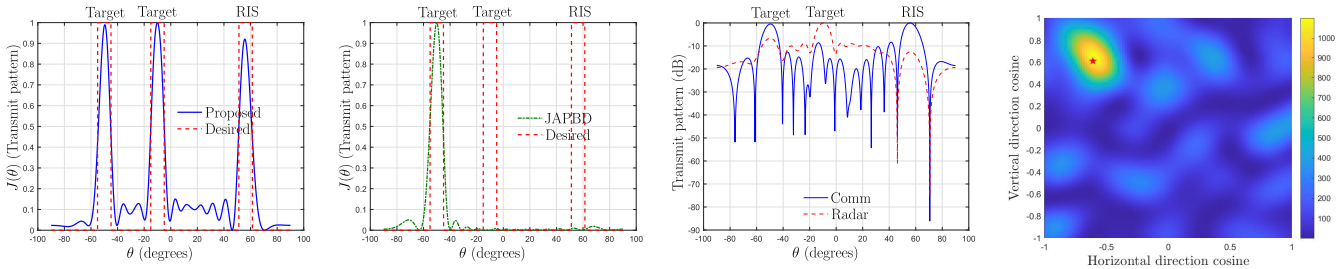

Fig. 3. (a) Transmit beampattern at the DFBS of the proposed method (b) Transmit beampattern at the DFBS of JAPBD [34] (c) Sensing and communication transmit beams viewed separately. (d) Reflection profile at the comm-RIS (`Proposed-D`). Star ($\star$) indicates the true location of the UE w.r.t. the RIS. (Both `Proposed-D` and `Proposed-F` results in the same transmit beampattern.).

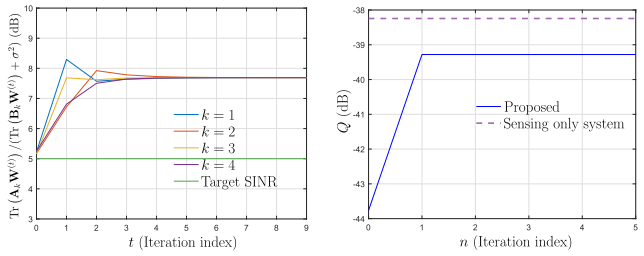

Fig. 4. (a) Convergence of iterations for updating $\boldsymbol{\omega}_{\mathrm{c}}$. (b) Convergence of Algorithm 1.

the `Proposed-D` provides significantly high SINR, without consuming any additional power. This is due to the fact that the selection of comm-RIS phase shifts is carried out to maximize the SINR itself, unlike the other schemes. Impact of Γ on the worst-case target illumination power is presented in Fig. 5(b). The worst-case target illumination power of `JAPBD` is significantly less than that of other schemes. This happens due to the choice of sum radar SNR as the performance metric in `JAPBD` which results in scenarios like the one presented in Fig. 3(a) wherein not all targets are illuminated. On the other hand, due to the use of a weighted sum of beampattern mismatch error and average squared cross-correlation as the radar metric, the radar performance of the rest of the schemes are much higher than that of `JAPBD`. Moreover, performance of `Proposed-D` is also comparable to that of a `sensing-only system`, which is the benchmark method since an ISAC system cannot achieve better sensing performance than a comparable sensing-only system. The worst-case target illumination power of `Proposed-D` is only about 1.5 dB worse than that of an ISAC system without the RIS. Let us recall that in the proposed methods, we are forming beams not only towards the target directions but also towards the comm-RIS. The formation of the additional beam towards the comm-RIS consumes additional power, which could otherwise be used to increase the target illumination power, leading to the reduced radar performance. At the same time, we observe that the communication performance in terms of worst-case SINR of the scheme with comm-RIS is significantly better than that of a scheme without RIS. Hence, there exists a tradeoff between the communication and sensing functionalities due to the presence of the additional beam towards the comm-RIS. We can also observe that the worst-case target illumination power of `no RIS` and `sensing-only system` are comparable as these do not form any beam towards the RIS.

In Fig. 5(c) and Fig. 5(d), we present the communication and radar performance of different methods for varying number of RIS elements. As before, SINR of `Proposed-D` is significantly higher than that of other benchmark schemes. The worst-case target illumination power of `Proposed-D` is also remarkably better than that of `JAPBD` and is comparable to that of the benchmark scheme `sensing-only system`. The fairness SINR of `Proposed-D` also increases with an increase in the number of comm-RIS elements due to the increased array gain offered by the RIS. On the other hand, since the comm-RIS is not involved in sensing, changes in N will not affect the worst-case target illumination power. Albeit a moderate loss of about 1.5 dB in Q due to the formation of an additional beam towards the RIS, the fairness SINR is significantly improved, often by more than 10 dB by properly designing $\boldsymbol{\omega}_{\mathrm{c}}$.

Next, we consider a setting where only K_d out of K users have a direct path from the DFBS and the direct paths to the remaining $K - K_d$ UEs are blocked. For the considered scenario, an ISAC system without RIS would only be able to serve K_d users out of K. We show the minimum-rate, i.e., $\min_k \log(1+\gamma_k)$ and the worst-case target illumination power for different number of UEs with direct path, i.e., K_d, in Fig. 5(e) and Fig. 5(f), respectively. We can see that with the comm-RIS, all the K users, irrespective of the presence of a direct path or not, is guaranteed a minimum SINR of $\Gamma = 5$ dB (or min-rate of 2.05 bps/Hz). However, without the RIS, only K_{d} users are served with an SINR higher than 5 dB. Although `RIS manual selection` and `JAPBD` also offer a min-rate of 2.05 bps/Hz, `Proposed-D` offers a significantly higher min-rate of about $4-8$ bps/Hz. As before, the value of Q of ISAC systems with RIS degrades by about $1.5 - 2.5$ dB compared to an ISAC system without RIS. We wish to re-emphasize that `JAPBD` often results in scenarios where not all targets are properly illuminated, leading to low values of the worst-case target illumination power, as indicated in Fig. 5(f). On the other hand, the proposed schemes ensures that all targets are illuminated with sufficient power even when the direct path to a few of the users is blocked. Throughout the simulations, we have also observed (not shown here) that the mean squared cross-correlation of the proposed

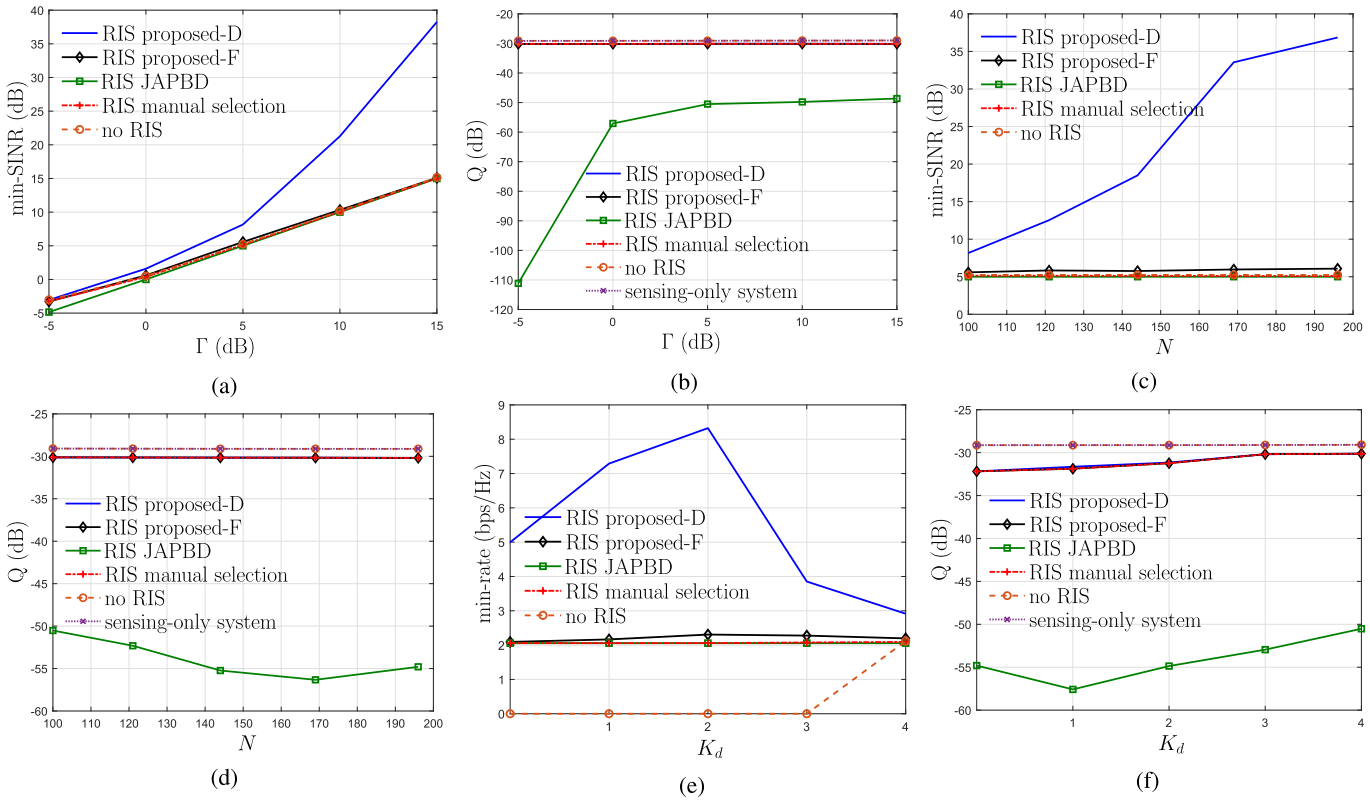

Fig. 5. Comm-RIS assisted ISAC system. Impact of Γ on (a) fairness SINR and (b) worst-case target illumination power. Impact of N on (c) fairness SINR and (d) worst-case target illumination power. Impact of K_d on (e) min-rate and (f) worst-case target illumination power.

methods are comparable, often better, than that of JAPBD scheme.

B. Dual RIS-Assisted ISAC System

In this subsection, we demonstrate the advantages of using dedicated RISs for sensing and communications in an ISAC system. We assume that two identical RIS with N elements assist the communication and sensing functionalities of the ISAC system. We use the same simulation parameters as before and the parameters are provided in Table II. Unless otherwise mentioned, we use $K = 4$, $T = 5$, $\Gamma = 5$ dB, $P_t = 0$ dB, and $N = 100$.

We begin by discussing the convergence of Algorithm 2. We present the convergence of iterations to update $\boldsymbol{\omega}_c$ and the overall Algorithm 2 in Fig. 6(a) and Fig. 6(b), respectively. We observe that the Dinkelbach iterations converge in a few (about 6) iterations. Similar to Algorithm 1, we can also observe that Q attains the maximum value in just 1 iteration.

Let us recall that the dual RIS-assisted ISAC system is particularly suited for scenarios where some or all of the targets are not directly visible to the DFBS. Let T_d denote the number of targets that are directly visible to the DFBS. In this section, we present the fairness SINR (or min-rate) and Q of different schemes for varying simulation parameters such as SINR constraints (Γ), number of RIS elements (N), number of users with direct path K_d, and the number of targets that are directly visible to the DFBS (T_d). All the results in this subsection are obtained by averaging over 100 independent channel realizations with varying user locations.

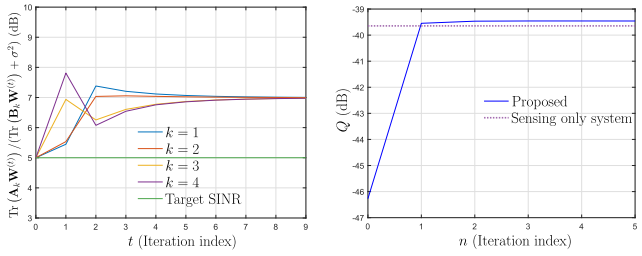

Fig. 6. (a) Convergence of iterations for updating $\boldsymbol{\omega}_c$. (b) Convergence of Algorithm 2.

As before, we compare the performance of the proposed methods, i.e., Proposed-D and Proposed-F, with that of manually designing beams at each RIS. Specifically, we select the radar-RIS (respectively, comm-RIS) phase shifts to form equally powerful beams towards all the targets locations of interest (respectively, all UEs). The transmit beamformers are then obtained by solving (30). We consider four different scenarios of ISAC systems for comparison: dual RIS with manually selected phase shifts to form interpretable beams, indicated as manual selection (both RISs); only single radar-RIS with manually designed phase shifts, indicated as manual selection (only radar RIS); only single comm-RIS with manually designed phase shifts, indicated as manual selection (only comm RIS); and ISAC system without RIS, indicated as no RIS. The methods with manual selection of RIS phase shifts are agnostic to the considered task. In addition, we also use

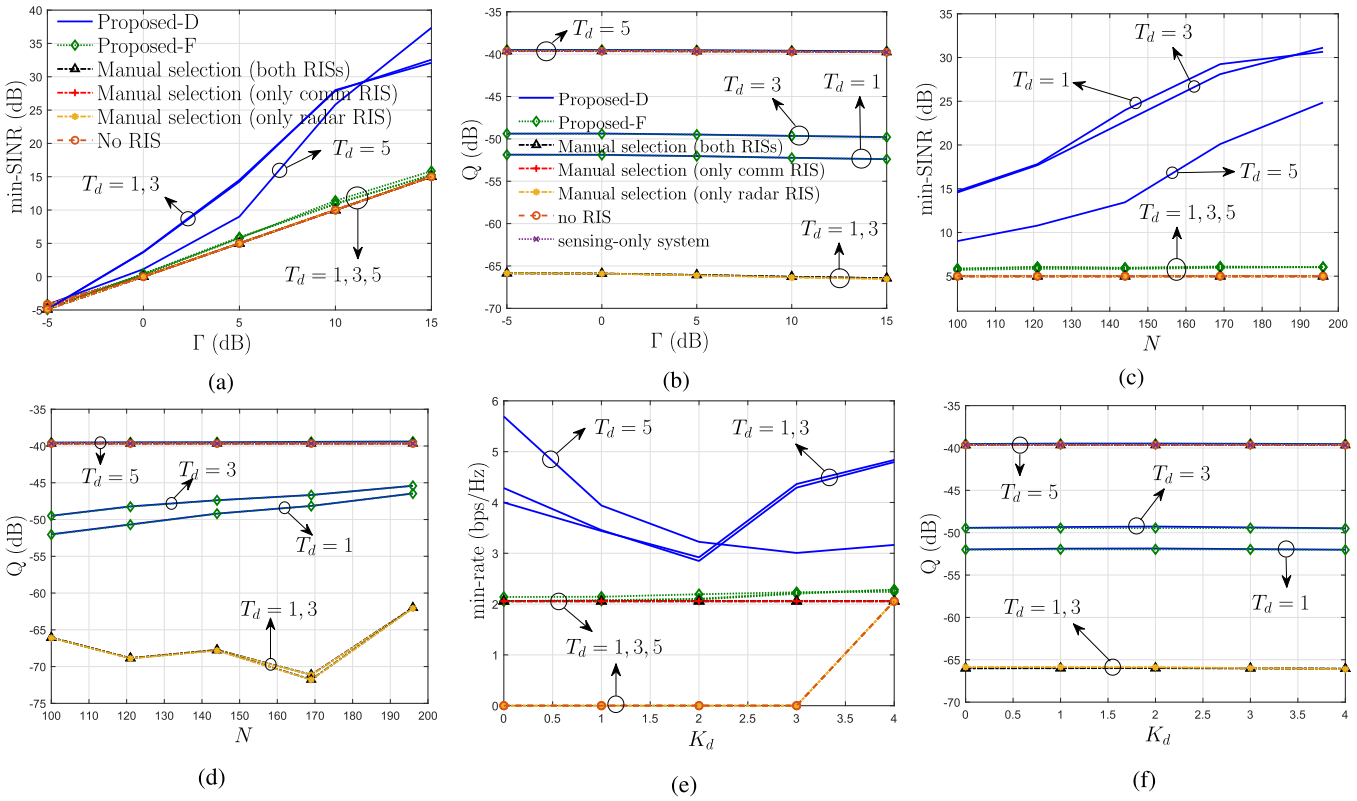

Fig. 7. Dual RIS-assisted ISAC system. Impact of Γ on (a) fairness SINR and (b) worst-case target illumination power. Impact of N on (c) fairness SINR and (d) worst-case target illumination power. Impact of K_d on (e) min-rate and (f) worst-case target illumination power.

`sensing-only system` [15] as a baseline system for radar performance.

In Fig. 7(a), we present the fairness SINR of different methods. `RIS proposed-D` clearly outperforms baseline systems based on manual selection of RIS phase shifts, ISAC system without RIS [12] and sensing-only system [15] while improving the fairness SINR by often more than 15 dB, irrespective of whether all targets are directly visible to the DFBS or not. Since the precoder design phase attempts to maximize Q while satisfying the fairness SINR, the fairness SINR will be about Γ. This is the reason why all the baseline methods achieve a fairness SINR of Γ dB. However, in `RIS proposed-D`, once the precoders $\mathbf{C}$ and $\mathbf{S}$ are designed, the comm-RIS phase shifts $\boldsymbol{\omega}_c$ are also updated so as to maximize the SINR. This leads to a significantly high fairness SINR for `RIS proposed-D`.

The worst-case target illumination power of different methods is presented in Fig. 7(b). As expected, schemes that do not utilize a dedicated radar-RIS are not able to illuminate all targets efficiently whenever a few targets (say, $T_d = 1, 3$) are not directly visible to the DFBS. While `manual selection (only radar RIS)` and `manual selection (both RISs)` results in a non-zero worst-case target illumination power, `RIS proposed-D` offers more than 12 dB higher Q than the next best benchmark scheme. As T_d increase from 1 to 3, the Q of `RIS proposed-D` also increase by about 3 dB. This is expected since more number of targets can be now served directly via the DFBS. When all targets are visible to the DFBS (i.e., $T_d = 5$), the performance of all methods are comparable with `RIS proposed-D` offering a slight improvement. Furthermore, in Fig. 7(b), we observe that Q of all schemes decrease with an increase in the SINR requirement. This is because of the higher amount of power that needs to be transmitted towards the UEs to meet the increased fairness SINR requirement.

In Fig. 7(c) and Fig. 7(d), we illustrate the impact of number of RIS elements (N) on the fairness SINR and worst-case target illumination power, respectively. As before, irrespective of the number of targets with direct paths, `RIS proposed-D` offers significant improvements in the fairness SINR over other benchmark schemes. Moreover, Q of `RIS proposed-D` is also remarkably high when compared with schemes where the radar-RIS phase shifts are manually designed, especially when few of the targets are not directly visible to the DFBS. As the number of radar-RIS (respectively, comm-RIS) elements increase, the array gain offered by the radar-RIS (respectively, comm-RIS) also increase leading to an increase in Q (respectively, fairness SINR). Since the comm-RIS is not involved in radar sensing, Q of `manual selection (only radar RIS)` and `manual selection (both RISs)` overlap with each other. Similarly, both `manual selection (only comm RIS)` and `no RIS` also have identical values of Q because both these scenarios correspond to a setting without the radar-RIS.

Finally, we show the performance of the proposed dual-RIS-assisted ISAC system in a scenario with the direct paths to a few of the users is blocked in Fig. 7(e) and Fig. 7(f). As before, with the use of the comm-RIS, all users are served

with a minimum SINR of 5 dB (i.e., min-rate of 2.05 bps/Hz). Moreover, with `RIS proposed-D`, all users are served with a higher rate irrespective of T_d. As can be observed from Fig. 7(f), `RIS proposed-D` results in remarkably improved worst-case target illumination powers, especially when the direct paths to a few of the targets are blocked. In sum, albeit the inability to form uncorrelated beams due to the fully passive nature of RISs, using an additional RIS for radar sensing along with the comm-RIS leads to significant improvements in both radar and communication performance of ISAC systems especially when not all targets are directly visible to the DFBS.

We remark that the behavior of the communication SINR (or rate) for different values of K_d and T_d is not monotone and is a consequence of the nature of the algorithm wherein we can only ensure that the resulting SINR is higher than the minimum required value. The exact value of SINR depends on the value selected for $\Gamma^{(n)}$ during the iterations as well as the quality of the solution obtained from the Gaussian randomization.

Moreover, throughout the simulations, we have observed that the performance of `Proposed-F` is also marginally better than that of other benchmark schemes in terms of the communication performance. Unlike [34], `Proposed-F` also ensures that all the targets are well illuminated. However, the communication performance of `Proposed-F` is still significantly less than that of `Proposed-D` since the latter (based on Dinkelbach iteration) designs $\boldsymbol{\omega}_c$ to maximize the fairness SINR itself instead only giving a feasible solution as is the case with `Proposed-F`.

While the single-RIS assisted ISAC system resulted in an improved communication performance at a cost of about 1-2 dB loss in the radar target illumination power, there is no such loss in radar performance for the setting with two RISs since the dual RIS-assisted ISAC can efficiently illuminate multiple targets and still guarantee a certain amount of SINR for all users even when neither the targets nor the users are directly visible at the DFBS. However, a disadvantage of the dual-RIS assisted ISAC system is its inability to form uncorrelated beams towards different target directions owing to the fully passive nature of the RIS array.

VII. Conclusion

We considered two settings of RIS-assisted ISAC systems, namely, a setting with a single RIS that assists only the communication functionality of an ISAC system and a setting with two RISs wherein dedicated RISs are used for sensing and communications. We developed algorithms to design the transmit beamformers to jointly precode communication symbols and radar waveforms and to also design RIS phase shifts to achieve certain sensing performance in terms of the beampattern matching error or worst-case target illumination power while ensuring a minimum SINR for the communication UEs. Since the resulting optimization problems are non-convex, we have developed alternating optimization solvers for the design problems that appear in the two settings. A semidefinite convex problem is used to solve for transmit beamformers with fixed RIS phase shifts. With fixed transmit beamformers, the design of comm-RIS phase shifts is carried out using generalized Dinkelbach iterations. With fixed transmit beamformers, the design of radar-RIS phase shifts is carried out using SDP followed by Gaussian randomization. The performance of the proposed algorithms is then demonstrated through numerical simulations. Specifically, the comm-RIS assisted ISAC system is found to significantly improve the fairness SINR while suffering from a moderate loss in radar performance. On the other hand, the dual-RIS assisted ISAC system is found to remarkably improve both communication and radar performance metrics, especially in scenarios where all the targets are not directly visible to the DFBS.

References

[1] N. Rajatheva et al., "White paper on broadband connectivity in 6G," 2020, *arXiv:2004.14247*.

[2] F. Liu et al., "Integrated sensing and communications: Toward dual-functional wireless networks for 6G and beyond," *IEEE J. Sel. Areas Commun.*, vol. 40, no. 6, pp. 1728–1767, Jun. 2022.

[3] H. Wymeersch et al., "Integration of communication and sensing in 6G: A joint industrial and academic perspective," in *Proc. IEEE 32nd Annu. Int. Symp. Pers., Indoor Mobile Radio Commun. (PIMRC)*, Helsinki, Finland, Sep. 2021, pp. 1–7.

[4] M. Nemati, Y. H. Kim, and J. Choi, "Toward joint radar, communication, computation, localization, and sensing in IoT," *IEEE Access*, vol. 10, pp. 11772–11788, 2022.

[5] W. Xu, Z. Yang, D. W. K. Ng, M. Levorato, Y. C. Eldar, and M. Debbah, "Edge learning for B5G networks with distributed signal processing: Semantic communication, edge computing, and wireless sensing," *IEEE J. Sel. Topics Signal Process.*, vol. 17, no. 1, pp. 9–39, Jan. 2023.

[6] K. V. Mishra, M. R. B. Shankar, V. Koivunen, B. Ottersten, and S. A. Vorobyov, "Toward millimeter-wave joint radar communications: A signal processing perspective," *IEEE Signal Process. Mag.*, vol. 36, no. 5, pp. 100–114, Sep. 2019.

[7] D. Ma, N. Shlezinger, T. Huang, Y. Liu, and Y. C. Eldar, "Joint radar-communication strategies for autonomous vehicles: Combining two key automotive technologies," *IEEE Signal Process. Mag.*, vol. 37, no. 4, pp. 85–97, Jul. 2020.

[8] A. R. Chiriyath, B. Paul, and D. W. Bliss, "Radar-communications convergence: Coexistence, cooperation, and co-design," *IEEE Trans. Cognit. Commun. Netw.*, vol. 3, no. 1, pp. 1–12, Mar. 2017.

[9] Z. He, W. Xu, H. Shen, Y. Huang, and H. Xiao, "Energy efficient beamforming optimization for integrated sensing and communication," *IEEE Wireless Commun. Lett.*, vol. 11, no. 7, pp. 1374–1378, Jul. 2022.

[10] L. Zheng, M. Lops, Y. C. Eldar, and X. Wang, "Radar and communication coexistence: An overview: A review of recent methods," *IEEE Signal Process. Mag.*, vol. 36, no. 5, pp. 85–99, Sep. 2019.

[11] F. Liu, C. Masouros, A. P. Petropulu, H. Griffiths, and L. Hanzo, "Joint radar and communication design: Applications, state-of-the-art, and the road ahead," *IEEE Trans. Commun.*, vol. 68, no. 6, pp. 3834–3862, Jun. 2020.

[12] X. Liu, T. Huang, N. Shlezinger, Y. Liu, J. Zhou, and Y. C. Eldar, "Joint transmit beamforming for multiuser MIMO communications and MIMO radar," *IEEE Trans. Signal Process.*, vol. 68, pp. 3929–3944, 2020.

[13] F. Liu, Y.-F. Liu, A. Li, C. Masouros, and Y. C. Eldar, "Cramér–Rao bound optimization for joint radar-communication beamforming," *IEEE Trans. Signal Process.*, vol. 70, pp. 240–253, 2022.

[14] J. Pritzker, J. Ward, and Y. C. Eldar, "Transmit precoder design approaches for dual-function radar-communication systems," 2022, *arXiv:2203.09571*.

[15] P. Stoica, J. Li, and Y. Xie, "On probing signal design for MIMO radar," *IEEE Trans. Signal Process.*, vol. 55, no. 8, pp. 4151–4161, Aug. 2007.

[16] E. Basar, M. Di Renzo, J. De Rosny, M. Debbah, M.-S. Alouini, and R. Zhang, "Wireless communications through reconfigurable intelligent surfaces," *IEEE Access*, vol. 7, pp. 116753–116773, 2019.

[17] M. Di Renzo et al., "Smart radio environments empowered by reconfigurable intelligent surfaces: How it works, state of research, and the road ahead," *IEEE J. Sel. Areas Commun.*, vol. 38, no. 11, pp. 2450–2525, Nov. 2020.

[18] H. Wymeersch and B. Denis, "Beyond 5G wireless localization with reconfigurable intelligent surfaces," in *Proc. IEEE Int. Conf. Commun. (ICC)*, Dublin, Ireland, Jun. 2020, pp. 1–6.

[19] S. Buzzi, E. Grossi, M. Lops, and L. Venturino, "Foundations of MIMO radar detection aided by reconfigurable intelligent surfaces," *IEEE Trans. Signal Process.*, vol. 70, pp. 1749–1763, 2022.
[20] F. Wang, H. Li, and J. Fang, "Joint active and passive beamforming for IRS-assisted radar," *IEEE Signal Process. Lett.*, vol. 29, pp. 349–353, 2022.
[21] W. Lu, B. Deng, Q. Fang, X. Wen, and S. Peng, "Intelligent reflecting surface-enhanced target detection in MIMO radar," *IEEE Sensors Lett.*, vol. 5, no. 2, pp. 1–4, Feb. 2021.
[22] X. Shao, C. You, W. Ma, X. Chen, and R. Zhang, "Target sensing with intelligent reflecting surface: Architecture and performance," *IEEE J. Sel. Areas Commun.*, vol. 40, no. 7, pp. 2070–2084, Jul. 2022.
[23] Z.-M. Jiang et al., "Intelligent reflecting surface aided dual-function radar and communication system," *IEEE Syst. J.*, vol. 16, no. 1, pp. 475–486, Mar. 2022.
[24] Y. He, Y. Cai, H. Mao, and G. Yu, "RIS-assisted communication radar coexistence: Joint beamforming design and analysis," *IEEE J. Sel. Areas Commun.*, vol. 40, no. 7, pp. 2131–2145, Jul. 2022.
[25] X. Song, D. Zhao, H. Hua, T. X. Han, X. Yang, and J. Xu, "Joint transmit and reflective beamforming for IRS-assisted integrated sensing and communication," in *Proc. IEEE Wireless Commun. Netw. Conf. (WCNC)*, Austin, TX, USA, Apr. 2022, pp. 189–194.
[26] R. S. P. Sankar, B. Deepak, and S. P. Chepuri, "Joint communication and radar sensing with reconfigurable intelligent surfaces," in *Proc. IEEE 22nd Int. Workshop Signal Process. Adv. Wireless Commun. (SPAWC)*, Lucca, Italy, Sep. 2021, pp. 471–475.
[27] R. Liu, M. Li, and A. L. Swindlehurst, "Joint beamforming and reflection design for RIS-assisted ISAC systems," in *Proc. 30th Eur. Signal Process. Conf. (EUSIPCO)*, Belgrade, Serbia, Aug. 2022, pp. 997–1001.
[28] Y. Li and A. Petropulu, "Dual-function radar-communication system aided by intelligent reflecting surfaces," in *Proc. IEEE Sensor Array Multichannel Workshop (SAM)*, Trondheim, Norway, Jun. 2022, pp. 1–6.
[29] R. Liu, M. Li, Y. Liu, Q. Wu, and Q. Liu, "Joint transmit waveform and passive beamforming design for RIS-aided DFRC systems," *IEEE J. Sel. Topics Signal Process.*, vol. 16, no. 5, pp. 995–1010, Aug. 2022.
[30] X. Wang, Z. Fei, Z. Zheng, and J. Guo, "Joint waveform design and passive beamforming for RIS-assisted dual-functional radar-communication system," *IEEE Trans. Veh. Technol.*, vol. 70, no. 5, pp. 5131–5136, May 2021.
[31] X. Wang, Z. Fei, J. Huang, and H. Yu, "Joint waveform and discrete phase shift design for RIS-assisted integrated sensing and communication system under Cramér–Rao bound constraint," *IEEE Trans. Veh. Technol.*, vol. 71, no. 1, pp. 1004–1009, Jan. 2022.
[32] Z. Zhu et al., "Intelligent reflecting surface assisted integrated sensing and communications for mmWave channels," 2022, *arXiv:2202.00552*.
[33] E. Shtaiwi, H. Zhang, A. Abdelhadi, and Z. Han, "Sum-rate maximization for RIS-assisted radar and communication coexistence system," in *Proc. IEEE Global Commun. Conf. (GLOBECOM)*, Madrid, Spain, Dec. 2021, pp. 1–6.
[34] M. Hua, Q. Wu, C. He, S. Ma, and W. Chen, "Joint active and passive beamforming design for IRS-aided radar-communication," *IEEE Trans. Wireless Commun.*, vol. 22, no. 4, pp. 2278–2294, Apr. 2023.
[35] W. Dinkelbach, "On nonlinear fractional programming," *Manage. Sci.*, vol. 13, no. 7, pp. 492–498, Mar. 1967.
[36] A. L. Swindlehurst, G. Zhou, R. Liu, C. Pan, and M. Li, "Channel estimation with reconfigurable intelligent surfaces—A general framework," *Proc. IEEE*, vol. 110, no. 9, pp. 1312–1338, May 2022.
[37] J.-P. Crouzeix and J. A. Ferland, "Algorithms for generalized fractional programming," *Math. Program.*, vol. 52, nos. 1–3, pp. 191–207, May 1991.
[38] Z.-Q. Luo, W.-K. Ma, A. M. So, Y. Ye, and S. Zhang, "Semidefinite relaxation of quadratic optimization problems," *IEEE Signal Process. Mag.*, vol. 27, no. 3, pp. 20–34, May 2010.

R. S. Prasobh Sankar (Graduate Student Member, IEEE) was born in Kerala, India, in 1997. He received the B.Tech. degree (with Gold medal) in electronics and communication engineering from the National Institute of Technology, Calicut, Kozhikode, India, in 2019. He is currently pursuing the Ph.D. degree with the Department of Electrical Communication Engineering, Indian Institute of Science, Bengaluru. His primary research interests include wireless communications, signal processing, array signal processing, and machine learning. He was a recipient of the Prime Minister's Research Fellowship (PMRF), Government of India, and the Qualcomm Innovation Fellowship (QIF).

Sundeep Prabhakar Chepuri (Member, IEEE) received the M.Sc. degree (cum laude) in electrical engineering and the Ph.D. degree (cum laude) from the Delft University of Technology, The Netherlands, in July 2011 and January 2016, respectively. He is currently an Assistant Professor with the Department of Electrical Communication Engineering, Indian Institute of Science (IISc), Bengaluru, India. His general research interests include mathematical signal processing, statistical inference, and machine learning applied to network sciences and wireless communications. He is an Associate Editor of IEEE SIGNAL PROCESSING LETTERS and IEEE TRANSACTIONS ON SIGNAL AND INFORMATION PROCESSING OVER NETWORKS.

Yonina C. Eldar (Fellow, IEEE) received the B.Sc. degree in physics and the B.Sc. degree in electrical engineering from Tel Aviv University (TAU), Tel Aviv, Israel, in 1995 and 1996, respectively, and the Ph.D. degree in electrical engineering and computer science from the Massachusetts Institute of Technology (MIT), Cambridge, MA, USA, in 2002. She was a Professor with the Department of Electrical Engineering, Technion—Israel Institute of Technology, Haifa, Israel, where she held the Edwards Chair in Engineering. She is currently a Professor with the Department of Mathematics and Computer Science, Weizmann Institute of Science, Rehovot, Israel. She is a EURASIP Fellow.